Agricultural and Forest Meteorology 373 (2025) 110731

Contents lists available at ScienceDirect

Agricultural and Forest Meteorology

journal homepage: www.elsevier.com/locate/agrformet

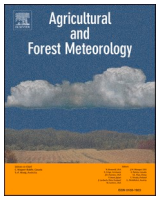

Cosmic-ray neutron sensors provide scale-appropriate soil water content and vegetation observations for eddy covariance stations in agricultural ecosystems

C. Brogi [a,1,*], J. Jakobi [a,1], J.A. Huisman [a], M. Schmidt [a], C. Montzka [a], J.S. Bates [a,b], S. Akter [a], H.R. Bogena [a]

[a] Agrosphere Institute (IBG-3), Forschungszentrum Jülich GmbH, 52425 Jülich, Germany
[b] Earth Observation and Ecosystem Modelling Laboratory (EOSystM) lab, SPHERES Research Unit, Université de Liège (ULiege), 4000 Liège, Belgium

ARTICLE INFO

Keywords:
Cosmic-ray neutron sensor
Soil water content
Gross primary productivity
Above ground biomass
Plant height
Leaf area index
Agricultural ecosystems

ABSTRACT

Continuous information on soil water content (SWC) and plant development is crucial for environmental monitoring, agricultural management, and beyond. Cosmic-ray neutron sensors (CRNS), widely used to estimate SWC, also have the potential to monitor field-scale variations in vegetation properties. In this study, a CRNS measured both epithermal (E_N) and thermal (T_N) neutron intensities over a 10-year period at an ICOS Class 1 ecosystem station in Selhausen (Germany). Compared to nearby point-scale sensors, the CRNS provided more representative SWC estimates within the monitoring area of the adjacent eddy covariance (EC) station. A general co-development was observed between T_N and gross primary productivity (GPP), but differences during senescence and desiccation suggest that factors beyond plant water content can influence T_N. An extensive dataset of plant height (PH), leaf area index (LAI), and dry above-ground biomass (AGB) was used to evaluate the ability of T_N to monitor plant development. T_N was found to be more closely related to vegetation dynamics than to changes in SWC. CRNS estimations of PH, LAI, and AGB yielded relatively good agreement with reference data (RMSE of 0.13 m, 1.01 m^2/m^2, and 0.27 kg/m^2, respectively). The RMSE obtained with a leave-one-out cross validation generally confirmed these findings. Although CRNS estimates generally had lower accuracy than traditional methods, they have the key advantages of being continuous, non-invasive, and non-laborious. Combined with simultaneous estimation of SWC at a relevant spatial scale, CRNS becomes a particularly interesting tool among long-term monitoring platforms with further potential in modelling, remote sensing, and decision-making in agriculture.

1. Introduction

Accurate and continuous monitoring of soil water content (SWC) and plant development offers significant benefits across a variety of environmental applications ranging from large-scale to smaller plot-level studies (Baret et al., 2007; Slingo et al., 2005). For instance, the integrated monitoring of these parameters is an essential component of long-term and continuous environmental observatories, such as the Integrated Carbon Observation System Research (ICOS) and the Integrated European Long-Term Ecosystem, critical zone and socio-ecological Research (eLTER) infrastructures (Ohnemus et al., 2024; Rebmann et al., 2018). Moreover, reliable SWC estimates and crop information such as plant height (PH), leaf area index (LAI), and above-ground biomass (AGB) are essential for testing and developing crop (Hao et al., 2024) and land surface models (Boas et al., 2021). At the same time, these monitoring efforts play a critical role in addressing practical challenges in agriculture (Biernacki and Bruton, 2000; Foley et al., 2011; Wang et al., 2019), where they can lead to higher yields, reduced

Abbreviations: AGB, above ground biomass; CRNS, cosmic-ray neutron sensor; EC, eddy covariance; E_N, epithermal neutron intensity; GAI, green area index; GNNS, global navigation satellite system; GPP, gross primary production; HDPE, high density polyethylene; LAI, leaf area index; LiDAR, light detecting and ranging; PH, plant height; RMSE, root mean square error; SWC, soil water content; T_N, thermal neutron intensity; UAS, unmanned aerial systems.

* Corresponding author.
E-mail address: c.brogi@fz-juelich.de (C. Brogi).
[1] C. Brogi and J. Jakobi contributed equally to this work.

https://doi.org/10.1016/j.agrformet.2025.110731
Received 29 January 2025; Received in revised form 19 May 2025; Accepted 5 July 2025
Available online 25 July 2025

agricultural inputs, and improved water use efficiency (Condon, 2020; Tardieu, 2022).

Generally, SWC is monitored using point-scale (e.g., time or frequency domain reflectometry) sensors or with remote sensing approaches (e.g., microwave sensors). A network of multiple point-scale sensors can improve the spatial representation of SWC variability (Bogena et al., 2010; Bogena et al., 2022b; Majone et al., 2013). However, such networks often underestimate SWC heterogeneity or misrepresent the average SWC of a given area (Western et al., 2002). Also, point-scale sensors may require frequent reinstallations, especially during agricultural activities. On the other hand, remote-sensing products often suffer from shallow penetration depths and limited spatio-temporal resolution, restricting their ability to capture SWC variability effectively (Mohanty et al., 2017; Wagner et al., 2007; Walker et al., 2004).

Estimating PH, LAI, and AGB generally involves in-situ measurements and destructive sampling. PH can be measured manually or via automated camera systems (Jiang et al., 2016; Wang et al., 2018). LAI is generally estimated by measuring light transmission through the canopy with portable sensors or hemispherical cameras (Bréda, 2003; Jonckheere et al., 2004; Wilhelm et al., 2000). AGB can be measured by drying harvested samples or using in-situ equipment such as weighted disks, pendulum sensors, or capacitance sensors (Catchpole and Wheeler, 1992; Serrano et al., 2016; Thoele and Ehlert, 2010). All these methods are resource-intensive, can be subjective, and may fail to characterize an entire field. Alternative methods that allow for large-scale measurements and are relatively automated include terrestrial laser scanning (Friedli et al., 2016), Unmanned Aerial Systems (UAS)-based Light Detecting and Ranging (LiDAR) measurements (Bates et al., 2021; Montzka et al., 2023; ten Harkel et al., 2019), and spectral and non-spectral remote sensing (Fang et al., 2019; Marshall and Thenkabail, 2015; Watanabe et al., 2017). Key shortcomings of these techniques include their generally non-continuous nature (Aranguren et al., 2020) and the need for optimal meteorological conditions (Wilhelm et al., 2000). This limits their ability to capture the full temporal dynamics of plant growth, particularly during extreme events like heat waves or prolonged droughts (Jakobi et al., 2018). Given the limitations of current methods, there is a pressing need for efficient and continuous field-scale monitoring of SWC and plant traits.

Cosmic-ray neutron sensors (CRNS) are increasingly popular SWC measurement devices that can fill the scale gap between in-situ sensors and remote sensing (Andreasen et al., 2017; Franz et al., 2013b; Zreda et al., 2012). Moreover, some studies investigated whether CRNS can be used to monitor vegetation dynamics or plant biomass at the field scale (Franz et al., 2013a; Jakobi et al., 2022; Togliatti and Hornbuckle, 2018). CRNS measure the intensity of environmental neutrons in the epithermal (~0.5 eV – 100 keV) or thermal (below ~0.5 eV) energy regime at approximately 1 m height. Generally, CRNS are equipped with one or more gas-filled counter tubes covered by a high-density polyethylene (HDPE) moderator that slows down epithermal neutrons and allows for their detection. These epithermal neutrons are primarily moderated by elastic collisions with hydrogen atoms, and the measured epithermal neutron intensity (E_N) is thus inversely proportional to the amount of water in the surrounding environment. As such, a single CRNS allows for the non-invasive determination of SWC (Desilets et al., 2010; Zreda et al., 2008) over a large detection volume (130 to 240 m radius and 15 to 83 cm soil depth, depending on SWC), making CRNS attractive compared to most other ground-based SWC sensors (Köhli et al., 2015; Schrön et al., 2017).

Besides SWC (Bogena et al., 2022b; Zheng et al., 2023), CRNS have been successfully used to determine snow dynamics (Bogena et al., 2020; Gugerli et al., 2019; Schattan et al., 2017), validate satellite-based SWC products (Babaeian et al., 2018; Montzka et al., 2017), support hydrological (Schattan et al., 2020; Shuttleworth et al., 2013) and land surface models (Baatz et al., 2017; Rosolem et al., 2014), and to investigate the role of infiltration on land-atmosphere feedback in land-atmosphere models (Arnault et al., 2024). To account for the influence of surrounding biomass on CRNS measurements (Baroni and Oswald, 2015; Tian et al., 2016), corrections have been developed to remove or reduce such vegetation influences on measured E_N, enabling more accurate SWC estimation(Al-Mashharawi et al., 2025; Baatz et al., 2015; Hawdon et al., 2014; Jakobi et al., 2018; Jakobi et al., 2022). These corrections are generally applied alongside other established corrections for air humidity (Rosolem et al., 2013), air pressure (Desilets and Zreda, 2003), and incoming cosmic-ray neutron intensity (Zreda et al., 2012). Typically, CRNS require low maintenance and provide continuous SWC measurements that are not affected by soil temperature (Zreda et al., 2008). This is especially useful in agricultural applications (Ragab et al., 2017), where a single CRNS does not hinder management practices (Franz et al., 2016) and thus has great potential for SWC monitoring to support irrigation management (Brogi et al., 2023; Finkenbiner et al., 2019; Li et al., 2019; Zhu et al., 2014). It is envisioned that the use of CRNS will increase in the coming years, thanks to the growing number of permanently installed CRNS, near-real time data availability, decreasing costs, and the availability of mobile measurement systems (Jakobi et al., 2020; McJannet et al., 2017).

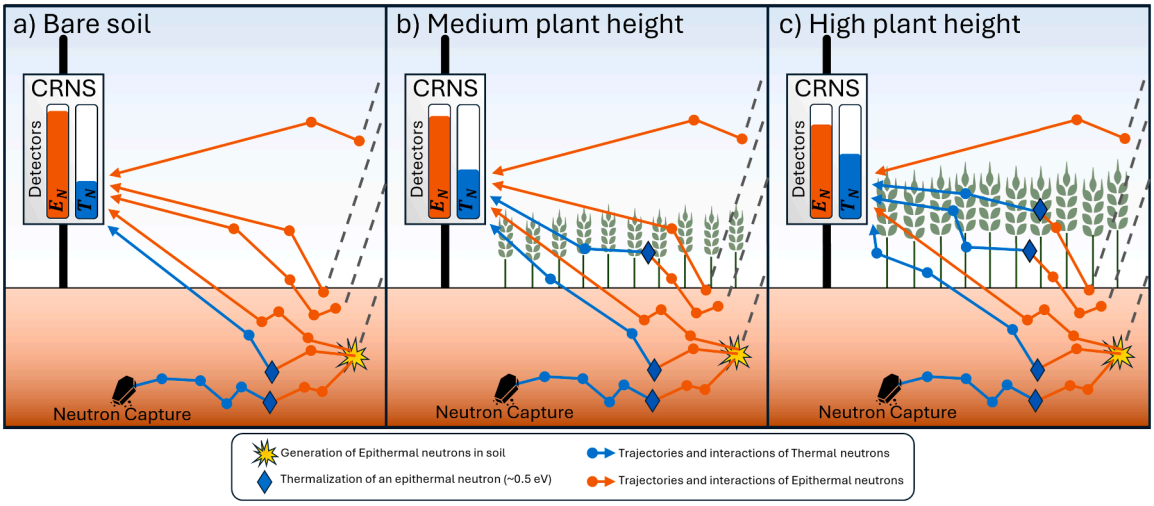

Fig. 1. Schematic representation of important soil and vegetation-related processes for thermal and epithermal neutrons for different plant conditions: a) bare soil, b) medium and c) high plant height, and qualitative indication of corresponding neutron count rates (i.e., coloured bars in the E_N, and T_N detectors). The thermalization of a neutron, i.e., the energy at which it enters the thermal energy regime from the epithermal energy regime, is set at ~0.5 eV.

Some CRNS are additionally provided with a bare counter tube that measures thermal neutron intensity (T_N). T_N also depends on the amount of hydrogen nuclei in the surroundings, but within a smaller detection radius of 43 to 48 m (Jakobi et al., 2021). Thermal neutrons have a higher probability of absorption due to their lower kinetic energy compared to epithermal neutrons, so that interaction processes above the soil surface (e.g. with vegetation) are of greater importance (Jakobi et al., 2022). Fig. 1 shows a schematic representation of important soil and vegetation-related processes for thermal and epithermal neutrons in different conditions (bare soil, medium, and high plant height). The corresponding impact on measured E_N and T_N is shown by the coloured filling of each detector. In the case of bare soil conditions or scarce vegetation (Fig. 1a), E_N is mostly related to SWC. With increasing vegetation cover (Fig. 1b-c), epithermal neutrons are increasingly moderated by vegetation biomass (Coopersmith et al., 2014; McJannet et al., 2014; Rivera Villarreyes et al., 2011), resulting in a decrease in E_N. Simultaneously, T_N increases with increasing vegetation biomass. This increase due to biomass is typically stronger than the decrease due to increasing SWC. Several studies have investigated the use of the neutron ratio (calculated from E_N *and* T_N) to correct SWC estimates or to estimate biomass water equivalent (Jakobi et al., 2018; Tian et al., 2016). More recently, Jakobi et al. (2022) suggested that T_N may be used to estimate AGB. Unfortunately, the effects of SWC and plant development co-varied in the study of Jakobi et al. (2022) and data were collected from three different fields under varying meteorological conditions. Thus, it cannot be excluded that local effects, such as different soil properties between the test sites, affected their results.

In this study, a single agricultural field with repetitions of four crops was monitored over an extended period (2015-2024). This minimizes external effects on the CRNS measurements, other than vegetation. The selected field is an ICOS Class 1 ecosystem station (Selhausen, DE-RuS) where SWC is monitored by point-scale sensors at five locations, while water and greenhouse gas fluxes are measured with the eddy covariance (EC) method. This setting provides a unique opportunity to explore potential synergies between CNRS measurements and the EC method, as both provide continuous measurements over an extensive field-scale area. The key goals of this study are to:

a) investigate and assess the possibility to use T_N to continuously monitor plant traits (i.e., PH, LAI, and dry AGB) at the field-scale;
b) assess whether the relationships between T_N and PH are stable for different crops or if there are crop-specific relationships between T_N and PH;
c) explore the added value of CRNS-based SWC and vegetation estimates for long-term environmental monitoring platforms like the Selhausen ICOS station.

To achieve these goals, SWC estimated by the CRNS was compared to estimates from the point-scale sensors. In doing this, the added value of the CRNS was investigated in light of its sensing volume, which is similar to that of the EC station. Then, T_N was visually compared with gross primary productivity (GPP) estimated by the EC station to identify similar patterns and crop-specific differences. An extensive dataset of PH, LAI, and dry AGB measurements was then used to develop and validate regression models for predicting plant traits from measured T_N, while additional UAS measurements were used to independently assess the CRNS-based estimations.

2. Materials and methods

2.1. Site and instrumentation

The experimental field is located near Selhausen (Fig. 2) in Germany, (50.866°N, 6.447°E). It is part of the Rur hydrological observatory (Bogena et al., 2018) within the TERrestrial ENvironmental Observatories (TERENO) infrastructure (Zacharias et al., 2024). The mean annual temperature and precipitation are 10.2°C and 714 mm, respectively (Korres et al., 2015). The main soil type is Luvisol (Rudolph et al., 2015), with soils composed of silty sediments of aeolian origin atop Pleistocene sand and gravel sediments of the Rhine/Meuse river system (Weihermüller et al., 2007). In the central part of the field, soils are relatively homogeneous with silty sediments extending beyond 2 m depth as indicated by the apparent electrical conductivity (ECa) maps in Fig. 2 (Brogi et al., 2019). The water table is rather shallow, typically ranging between 2.0 and 2.6 m depth throughout the year (Brogi et al., 2021). The most common crops grown in rotation on the experimental field are winter cereals (winter wheat and winter barley), potatoes, and sugar beet.

At the centre of the experimental field, meteorological measurements were recorded by the Selhausen ICOS class 1 station starting in

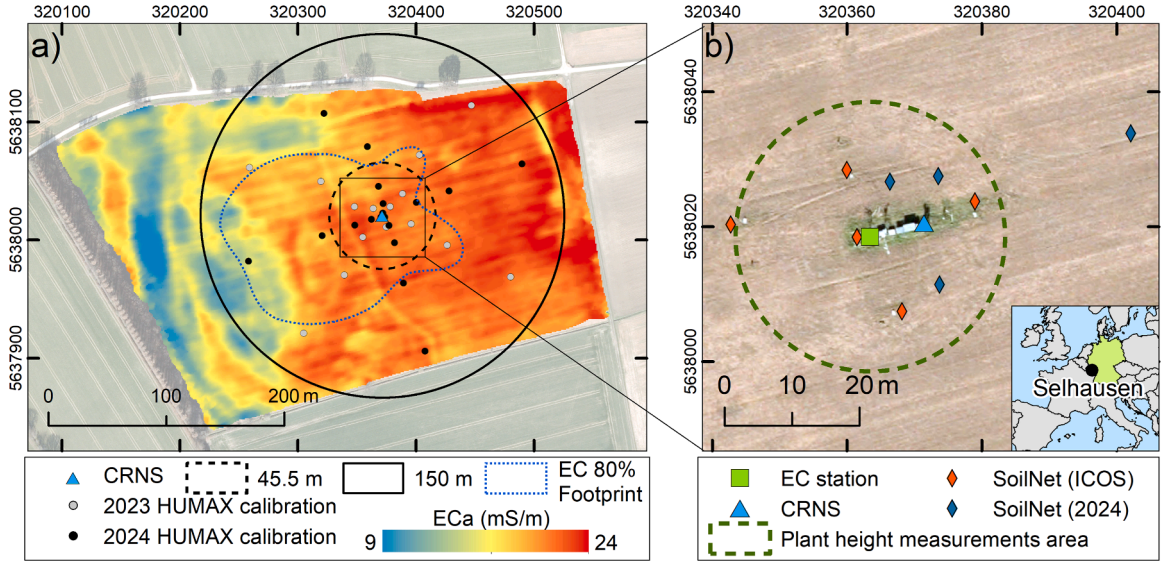

Fig. 2. Map of the investigated field with a) locations of the CRNS and soil sampling locations, b) the SoilNet wireless sensor network (ICOS-related and additional 2024 sensors), and EC station. The epithermal and thermal neutron footprint radii (i.e., 154 m and 45.5 m, respectively), the 80 % footprint of the EC station, and the area where plant height measurements were collected are shown with lines. The background of panel a) shows the apparent electrical conductivity (ECa) of the soil (Brogi et al., 2019). Both panels show a satellite image of the area (ESRI, 2024). The reference system is UTM Zone 32 North.

2019 (Schmidt et al., 2023). Before this, meteorological data were provided by a similar station that was part of the TERENO network (Bogena et al., 2018). Air temperature and relative humidity were measured with a HC2S3 sensor (Rotronic, Bassersdorf, Germany) and were used to calculate absolute humidity. Air pressure was measured with a PTB110 barometer (Vaisala Inc., Helsinki, Finland). Precipitation was recorded by a 200 cm^2 OTT Pluvio^2 weighing rain gauge (Ott HydroMet, Kempten, Germany) located ~300 m north-east of the experimental site. To measure key variables for the determination of eddy covariance fluxes, the Selhausen ICOS Class 1 ecosystem station is equipped with a 3D ultrasonic anemometer (HS-50, Gill Instruments Limited, Lymington, UK) and a closed-path infrared gas analyser (LI-7200, LI-COR Environmental, Lincoln, NE, USA). In contrast, the pre-ICOS EC setup featured a 3D ultrasonic anemometer (CSAT3, Campbell Scientific, Logan, UT, USA) and an open-path infrared gas analyser (LI-7500, LI-COR Environmental, Lincoln, NE, USA). Measurement heights of 2.6 m (ICOS) and 2.3 m (TERENO) were selected to ensure that flux measurements capture at least 70 % of the cumulative contribution from the target area, both during day- and nighttime.

A SoilNet wireless sensor network (Bogena et al., 2022b) with five measuring stations (i.e. end devices) in a radius of about 30 m around the CRNS was used to obtain reference SWC information (Fig. 2). Each SoilNet end device was equipped with five SMT100 SWC sensors (Trübner GmbH, Neustadt, Germany) installed at depths of 0.05, 0.10, 0.20, 0.50, and 1.00 m. In 2024, four additional SoilNet devices were placed at distances between 5 and 30 m from the CRNS and at depths of 5, 10, and 20 cm after seeding of sugar beet. Before installation, all sensors were individually calibrated to convert the raw sensor output to dielectric permittivity (Bogena et al., 2017), which was subsequently related to SWC using the Topp equation (Topp et al., 1980). During each major agricultural management activity (e.g., tillage, seeding, and harvest), these point-scale sensors were removed and then reinstalled. Finally, a CRS-1000 neutron detector (Hydroinnova LLC, Albuquerque, NM, USA) was installed in 2015 next to the EC station (Figs. 2 and B1). This CRNS was equipped with a moderated and a bare neutron counter to measure E_N and T_N, respectively.

2.2. Calibration of the CRNS and weighting of in-situ sensors

The SWC estimates derived from measured E_N require appropriate calibration with gravimetric SWC [g/g], soil bulk density (ρ_{bd} [g/cm^3]), and the sum of hydrogen stored in lattice water and soil organic carbon (θ_{off} [g/g]). Two soil sampling campaigns were conducted on 9th September 2023 and 28th June 2024. In both campaigns, 18 soil cores of 30 cm depth and with 5 cm diameter were collected using a HUMAX soil corer (Martin Bruch AG, Rothenburg, Switzerland). Soil sampling locations used for calibration were radially distributed to match the horizontal sensitivity of the CRNS (Schrön et al., 2017), and to better capture the field heterogeneity (Fig. 2). The soil cores were stored in a refrigerator until they were divided into 5 cm long segments and oven-dried at 105°C for 24 hours to obtain gravimetric SWC and ρ_{bd}. θ_{off} was obtained from a set of 18 samples obtained using the same sampling strategy on the 5th June 2015. For each sample, 20 mg of depth-specifically mixed soil was sieved and burned at 1000°C and θ_{off} was determined from the ignition weight loss.

Since a CRNS shows decreasing sensitivity with increasing distance from the sensor (Köhli et al., 2015; Schrön et al., 2017), the 18 soil sampling locations must be weighted to allow an accurate calibration of the CRNS measurements. An extensive description of the weighting procedure can be found in Schrön et al. (2017). In short, a vertical weighting was applied to the SWC, ρ_{bd}, and θ_{off} measurements by using the average depth (i.e., 2.5, 7.5, 12.5, 17.5, 22.5 and 27.5 cm) of the HUMAX samples. As the soil sampling locations were radially distributed according to the horizontal sensitivity of CRNS (Schrön et al., 2017), a horizontal weighting was implicitly applied. Thus, a double weighting was avoided by averaging first the measurements in each radius and then by averaging the results of these radii, resulting in vertically and horizontally weighted values. For ρ_{bd}, values from the 2023 and 2024 campaigns were averaged to obtain a single calibration value. As a comparison of soil organic carbon values in 2015 and 2018 (Saby et al., 2024) did not show consistent variations for the investigated field, the soil organic carbon content was assumed to be rather constant. Thus, θ_{off} determined in 2015 were used for both the 2023 and 2024 calibrations. Continuous in-situ SWC measured by the SoilNet sensors were also vertically and horizontally weighted according to the procedures suggested by Schrön et al. (2017) to obtain a weighted average SWC time series that can be compared to SWC estimated by the CRNS.

2.3. Processing of CRNS data and conversion to SWC

Raw E_N measured by the moderated detector and raw T_N measured by the bare detector of the CRNS were aggregated to hourly values (N_{raw}). In both cases, the following threshold values were applied as a first filter for outliers:

$$N_{c1} = \begin{cases} N_{raw} > 250 \dfrac{cts}{h} \\ N_{raw} < 1010 \dfrac{cts}{h} \end{cases} \quad (1)$$

where N_{c1} is the neutron intensity corrected for extreme outliers. Subsequently, outliers relative to the 24-hours moving average (N_{c24m}) ± the square root of the 24-hours moving sum ($\sqrt{N_{c24s}}$) were removed using:

$$N_c = \begin{cases} N_{c1} > N_{c24m} - \sqrt{N_{c24s}} \\ N_{c1} < N_{c24m} + \sqrt{N_{c24s}} \end{cases} \quad (2)$$

where N_c is the measured neutron intensity after outlier values were removed.

At each time step, the measured N_c must be corrected for environmental variables before it can be converted into SWC (Desilets and Zreda, 2001). The correction factor for variations in air pressure f_p was obtained using the approach from Desilets and Zreda (2003):

$$f_p = \exp\left(P_0 L - P\right) \quad (3)$$

where P is the measured air pressure [mbar], P_0 is the average pressure over the investigation period [mbar], and L [g/cm^3] is the local mass attenuation length, which decreases with latitude and was set to 131.6 g/cm^3 in this study. The correction factor for the variation of incoming cosmic-rays neutron intensity f_i was obtained using the method from Zreda et al. (2012):

$$f_i = \frac{I_{ref}}{I} \quad (4)$$

where I [cts/h] is the neutron intensity recorded by the Jungfraujoch (JUNG) neutron monitor in Switzerland (available at www.nmdb.eu). The JUNG neutron monitor was selected because it is known to provide high-quality and long-term data that can be used across Europe due to its central location (Bogena et al., 2022a; McJannet and Desilets, 2023). I_{ref} [cts/h] is an arbitrary reference value that was set to 150 cts/h, which was the average value of I on the 4th of March 2015 (starting date of CRNS measurements). The correction factor for the variation in atmospheric water vapour f_h was obtained using the method from Rosolem et al. (2013):

$$f_h = 1 + 0.0054(h - h_o) \quad (5)$$

where h is the measured absolute air humidity [g/cm^3] and h_o [g/cm^3] is the average air humidity over the investigation period. The corrected neutron intensity N was finally obtained by multiplying N_c with these

correction factors:

$$N = N_c{*}f_p{*}f_i{*}f_h \quad (6)$$

It should be noted that the most appropriate way to correct T_N is currently still being investigated (Andreasen et al., 2023; Desilets et al., 2010; Jakobi et al., 2018; Jakobi et al., 2022; Rasche et al., 2023; Schrön et al., 2024). Therefore, the corrected thermal neutron intensity was obtained either by using only the humidity and pressure correction ($T_{N_{p,h}}$), as suggested in Jakobi et al. (2018), or by including the incoming neutron correction instead(T_N). Additionally, a new approach for the correction of the humidity proposed by Rasche et al. (2023) was tested (see Appendix A).

For corrected E_N, a centred 24-hour running average was applied (Zreda et al., 2008) as this is the established method to reduce noise and measurement uncertainty in CRNS (Bogena et al., 2022a; Zreda et al., 2008; Zreda et al., 2012). To reduce the inherent uncertainty of corrected T_N, hourly measurements were aggregated to daily values and further smoothing was applied using a 3-day rolling mean. These measures were taken to obtain more reliable estimates of SWC and plant traits (Jakobi et al., 2020; Knoll, 2010).

Finally, volumetric SWC (θ) was obtained from E_N using the well-known N_0-approach (Zreda et al., 2012):

$$\theta = \rho_{bd}\left(\frac{p_0}{\frac{E}{N_0} - p_1} - p_2 - \theta_{off}\right) \quad (7)$$

where the parameters p_0, p_1, and p_2 are set to 0.0808, 0.3720, and 0.1150 as indicated by neutron transport modelling (Desilets et al., 2010), and N_0 is the epithermal neutron intensity above dry soil. In the calibration process, Eq. (7) is solved for N_0 using the SWC obtained from the HUMAX soil samples (described in section 2.2) and the average of E_N on the sampling day.

2.4. Estimation of gross primary productivity at the ICOS and TERENO EC station

For the period from 2019 to 2024, half-hourly GPP data from the Selhausen ICOS station provided by the ICOS Carbon Portal (Schmidt, 2024) were utilized. Specifically, the reference variable for gross primary production (GPP_NT_VUT_REF) was employed, which is derived using the methodology of Vitale et al. (2020) and Pastorello et al. (2020). Before 2019, GPP was derived from the pre-ICOS EC station, which started operation in 2011. In this case, fluxes were calculated using the 'TK3.1' software package (Mauder and Foken, 2015) following the strategy presented in Mauder et al. (2013). GPP was determined using the ReddyProc R package (Wutzler et al., 2018). Half-hourly GPP values from both datasets were aggregated into daily sums. The methodology for determining GPP at the two stations is largely congruent and systematic deviations that could distort the interpretation of the results are not expected for this specific study.

2.5. Vegetation measurements

Manual measurements of PH during the growing season were generally performed weekly within 20 m of the CRNS (green dashed circle in Fig. 2b). Each time, five randomly selected representative locations were used, avoiding areas where crop development differed significantly from most of the experimental field (e.g., tractor lanes). PH was measured with a ruler by recording the height of the top of the canopy at each location. LAI was measured at four fixed plots located 15 to 20 m from the CRNS using a SS1 SunScan Canopy Analysis System (Delta-T Devices Ltd, Burwell, UK) following the ICOS instructions for ancillary measurements. A total of 46 LAI estimates were available starting in late 2017, and the number of estimates per growing season ranged from three to ten.

To provide UAS-based high-resolution independent PH and Green Area Index (GAI) measurements, 27 PH campaigns (7 in 2020, 9 in 2021, 4 in 2022, and 7 in 2023) and 34 GAI campaigns (9 in 2020, 11 in 2021, 5 in 2022, and 9 in 2023) were carried out by using two DJI Matrice 600 (DJI, Shenzhen, China) UAS. Accurate positioning of the UAS was obtained in post-processing using an external Septentrio Altus NR3 (Septentrio, Leuven, Belgium) Global Navigation Satellite System (GNSS). For PH measurements, a YellowScan® Surveyor LiDAR (YellowScan, Saint-Clément-de-Rivière, France) was used at an altitude of 50 m above ground (precision of approximately 0.04 m). The field of view was limited to 70° (+-35° off-nadir) to remove unfavourable view angles. Then, a 0.15 m grid was created, and PH was determined from the difference between the highest and lowest points in each grid cell. Additional information on the methodology and measurements can be found in Montzka et al. (2023). For GAI, a Micasense RedEdge-M five-band multispectral camera and a Downwelling Light Sensor (DLS) for sun and cloud post-processing corrections were used at a height of 100 m above ground (resolution of the resampled grid of 0.15 m). GAI was calculated via the Normalized Differenced Vegetation Index (NDVI) following the approach of Ali et al. (2015) with further details found in Bates et al. (2021) and Brogi et al. (2020). Finally, PH and GAI values were averaged over a 45 m radius to match the expected thermal neutron footprint (see Fig. 2).

Destructive dry AGB measurements were collected at different locations within the ICOS field. These locations may occasionally be outside the EC and CRNS footprint, but due to the relatively low heterogeneity of the ICOS field, they represent a field-average value that can be used either with the EC station or with the CRNS. Dry AGB of winter barley at five dates in 2016 were obtained from the dataset of Reichenau et al. (2020). At each date, biomass was determined at three different locations in the investigated field and plants were collected from three different rows (each 40 or 50 cm wide). The dry AGB was determined by drying the collected plants in a drying oven at 105°C for at least three days. Furthermore, four destructive measurements of dry AGB for the investigated period were retrieved from the ICOS Carbon Portal (Schmidt, 2024). These measurements were obtained from samples taken at 24 locations distributed within the field. At each location, winter wheat plants from a 2 × 1 m row were collected whereas, for sugar beet and potato, 3 plants from two neighbouring rows were collected. Additionally, five destructive measurements of sugar beet dry AGB were performed in 2024 by visiting 4 to 6 locations per date. In this case, 4 to 6 plants per location were collected. For both the ICOS and the 2024 measurements, the dry AGB was determined by drying the collected plants in a drying oven at 65°C for at least three days following ICOS standards. In all these different campaigns, the number of plants per square meter was calculated based on row spacing and plant density.

2.6. Determination of PH, LAI, and dry AGB from thermal neutrons

Periods in which the field was in bare soil conditions or was covered with harvest residues were excluded from the analysis of T_N – plant traits relationships. Intercropping periods were also excluded since very limited information was available regarding the cover crops that generally have low PH and are a mixture of different plant species. In the case of winter barley and winter wheat, the winter months that precede stem elongation were also excluded from the analysis as, in this stage, crops are rather small and show little growth. In the analysed periods, PH [m] was estimated from thermal neutron intensities (T_N) by means of linear regression models:

$$PH_{T_{N_a}} = a{*}T_{N_a} + b \text{ and } PH_{T_N} = c{*}T_N + d \quad (8)$$

where a, b, c, and d are calibration parameters. Here, $PH_{T_{N_a}}$ [m] and PH_{T_N} [m] are the PH estimated from thermal neutrons where the thermal neutron intensity was normalized using two different approaches.

$PH_{T_{N_a}}$ used a normalized T_{N_a} obtained with the average of the whole measurement period ($\overline{T_{N_a}}$), whereas PH_{T_N} used a normalized T_N that was obtained for each separate growing season by using the average values from the 15th to the 17th of March of the given season ($\overline{T_N}$). These dates were selected as they precede the emergence of sugar beet and potato, while winter cereals generally showed a relatively low and constant PH. An exception was the spring of 2024 where intense and continuous precipitation prevented agricultural management and delayed seeding of sugar beet considerably until 1st May 2024. Here, the average value from 26th to 28th of April 2024 (five days before sowing) was used. Three different approaches were used to estimate PH_{T_N}: a) an all-crops model using the available growing seasons, b) crop-specific models where seasons with the same crop were aggregated, and c) annual models separating each of the nine growing seasons. The $\overline{T_{N_a}}$ normalization approach (resulting in $PH_{T_{N_a}}$) was only used in the all-crops model while the $\overline{T_N}$ normalization approach (resulting in PH_{T_N}) was used in all three approaches. By not using the T_{N_a} normalization approach for crop-specific and annual models, these are made more independent from T_N measured in different years. Due to the relatively low number of LAI and dry AGB measurements, only crop-specific linear relationships between T_N and LAI and annual relationships between T_N and dry AGB were established to estimate LAI_{T_N} and dry AGB_{T_N}. An exception is LAI_{T_N} estimates for winter wheat, for which two separate relationships were established (one for 2018 and 2020, and one for 2023).

Estimates of PH_{T_N}, LAI_{T_N}, and dry AGB_{T_N} were compared to measured values by means of visual inspection and through the root mean square error (RMSE). Additionally, the RMSE between estimated PH_T and measured PH, as well as the RMSE relative to the maximum PH, were used to quantify model quality. The intercept, slope, and respective confidence intervals of a) the all-crops model, b) the crop-specific models, and c) the annual models were used to compare the developed $T_N - PH$ relationships and to evaluate the extent to which the annual models can be replaced by more general approaches. Finally, T_N-based estimates were validated using a leave-one-out cross validation (LOOCV). The LOOCV RMSE, which is the square root of the mean squared prediction error obtained by leaving out one measurement at a time, was calculated for the crop-specific PH_{T_N} and LAI_{T_N} estimates. In the case of dry AGB_{T_N}, the LOOCV RMSE was calculated only for the years 2016 and 2024 as these were the only two years with sufficient manual measurements for validation.

3. Results and discussion

3.1. Long-term co-located CRNS and EC measurements

The filtering of outliers applied to measured epithermal (E_N) and thermal neutron intensities (T_N) resulted in the removal of 1.6 and 1.3 % of E_N and T_N values, respectively. Fig. 3 provides an overview of precipitation, E_N, T_N, SWC, and crop rotation for the investigated period. Fig. 3b shows the dynamics of E_N during the investigated period, which ranged from 471 to 773 cts/h, with an average of 600 cts/h. The analysis of the in-situ soil samples for the calibration of the CRNS resulted in $\rho_{bd} = 1.3$ g/cm^3, $\theta_{off} = 0.024$ m^3/m^3, and a N_0 of 1016 cts/h. This N_0 was the result of the two calibration values of SWC, which were 0.255 m^3/m^3 in September 2023 and 0.246 m^3/m^3 in June 2024. Fig. 3c shows the SWC estimated using E_N (black line) and the vertically and horizontally weighted point-scale SoilNet measurements (blue line). Overall, the temporal SWC dynamics from the CRNS and the weighted SoilNet measurements are in good agreement. However, the absolute SWC values obtained with CRNS do not match the weighted SoilNet measurements in some periods. This is also reflected by a relatively high overall RMSE of 0.063 m^3/m^3.

The observed discrepancy in SWC is attributed to several factors. First, the SoilNet sensors are installed in the proximity to the CRNS. Their weighted SWC represents an area within a maximum of about 15 m from the CRNS with the devices installed in 2019. This area was extended to about 30 m with the additional 4 devices installed in 2024 (see Fig. 1). In such conditions, distributed point-scale sensors can provide weighted SWC estimates that differ significantly from the CRNS estimate, which covers a much larger area (Brogi et al., 2023; Rasche et al., 2021; Schrön et al., 2022). Moreover, the in-situ SWC sensor measurements are disturbed by removal and reinstallation, such as

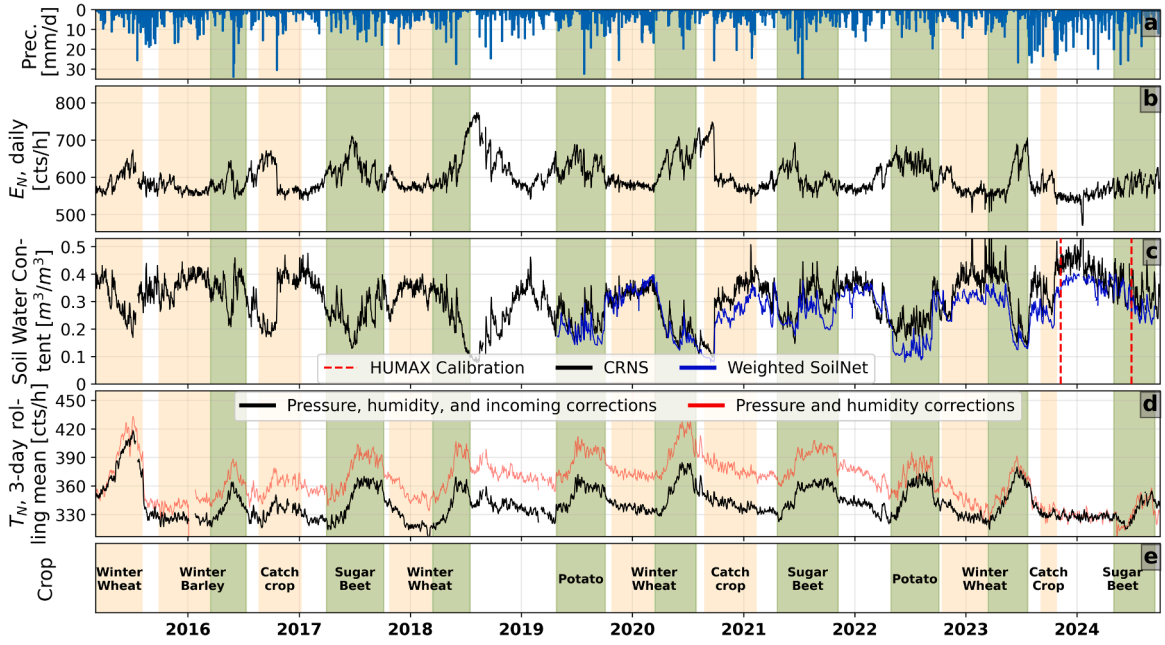

Fig. 3. Time series from the investigated site showing a) precipitation, b) E_N, c) SWC estimated from E_N (black) and reference SWC (blue) from the averaging of the SoilNet sensors, d) T_N with (red) and without (black) correction for incoming cosmic-ray neutrons, and e) crop rotation. The green areas indicate the investigated periods, whereas yellow areas indicate vegetated periods that are not included in the analysis.

before seeding or after harvest. For example, at the beginning of the 2022 potato season (Fig. 3c), the weighted SWC obtained from SoilNet shows a large drop, while CRNS estimates remain stable. This discrepancy persists throughout the growing season and may be related to the inherent difficulties of distributing point-scale sensors in a representative way over the high soil roughness created by the potato ridges. Also, the loose soil of the potato ridges can lead to the loss of direct contact of the in-situ sensors. These are probably the main reasons for the underestimation shown by the weighted SoilNet SWC and for the high RMSE of 0.090 m^3/m^3 in the 2022 potato season. This example shows the potential advantage of CRNS, which is not affected by these measurement challenges caused by land management. It should be noted that E_N was not corrected for biomass effects in this study. As it is known that biomass can affect E_N and thus SWC estimates (Baatz et al., 2015; Franz et al., 2013a; Jakobi et al., 2022), it cannot be excluded that part of the discrepancies in SWC between CRNS estimates and weighted SoilNet is due to the absence of a biomass correction. However, it is expected that a biomass correction would not be sufficient to compensate the described discrepancies, especially for periods like the 2022 potato season, because the biomass of an agricultural environment has a small impact on T_N compared to other ecosystems like forest. Moreover, it was not possible to achieve a comprehensive biomass correction for this specific study given the variety of crops, the number of growing seasons, and the limited amount of destructive biomass measurements.

The thermal neutron intensity (Fig. 3d) ranged between 271 and 435 cts/h (average of 365 cts/h) when corrected only for pressure and humidity ($T_{N_{p,h}}$), while it was between 304 and 418 cts/h (average of 345 cts/h) when also corrected for incoming neutrons (T_N). Fig. 3d shows a positive trend in $T_{N_{p,h}}$ until summer 2020, followed by a negative trend. This long-term fluctuation is related to the periodically occurring 11-year solar cycle (Balasubrahmanyan, 1969) and is minimized in T_N by correcting for incoming cosmic radiation. Although these results show that measured T_N should be corrected for incoming cosmic-ray neutrons, the applicability of the correction methods in equations (3-5) for thermal detectors should be further evaluated in future studies (Andreasen et al., 2023; Rasche et al., 2023). In the 2015 winter wheat growing season, T_N showed exceptionally high values related to the temporary presence of several moderated CRNS with HDPE moderators in the direct vicinity of the investigated CRNS (Fuchs, 2016; Jakobi et al., 2022), as shown in Appendix B (Fig. B1c). The presence of additional HDPE led to further moderation of ambient epithermal neutrons and a general increase in T_N of ~ 8% compared to the following years. Thus, the 2015 season was excluded from subsequent analysis. These aspects are further discussed in Appendix B (Fig. B2).

From the comparison of Figs. 3c and 3d, it is apparent that the dynamics of SWC and T_N are generally not consistent. Prominent examples include the sharp decreases in SWC (and thus an increase in E_N) at the end of the winter wheat growing season in 2018 and in the second half of the sugar beet growing season in 2021. Both are not reflected in the T_N measurements, which remained relatively constant. Similarly, the increases in SWC at the end of the sugar beet growing season in 2017 and at the beginning of the 2020-2021 catch crop growing season were not associated with changes in the T_N measurements. This indicates that T_N is not strongly influenced by surrounding SWC.

Fig. 4 shows T_N measured by the CRNS (Fig. 4a), manual PH measurements (Fig. 4b), and daily GPP estimates from the EC station (Fig. 4c). A comparison of T_N and PH, the latter including the stems that are left after harvest, shows that seasonal variations in T_N align with typical crop development patterns. For instance, the minimum T_N corresponds to periods when PH $\leq$ ~20 cm. However, the minimum T_N values vary across growing periods, likely due to management practices such as tillage and soil preparation, or drought conditions. Also, winter crops (barley and wheat) maintain a height of 10 to 20 cm until mid-March, during which the influence of hydrogen pools like SWC may outweigh biomass effects on T_N. An exception occurred during an uncultivated period between July 2018 and May 2019. As shown in Fig. 3d, an initial drop in T_N was followed by an increase, and then by a rather gradual decrease of T_N. During this period, SWC gradually recovered from exceptionally low values (Fig. 3c) that were the consequence of a heatwave across northern and central Europe (Beillouin et al., 2020; Graf et al., 2020) but there is no apparent co-development between SWC and T_N (Fig. 3c-d). Although it may be argued that effects other than SWC and biomass influenced T_N, it is not possible to provide clear interpretations from the available data for this relatively short period.

Fig. 4c shows daily GPP values measured during the operation of the TERENO EC station (blue lines), and those measured following the establishment of the ICOS Class 1 station (orange lines). Similar to the relationship between T_N and PH, T_N and GPP exhibit comparable

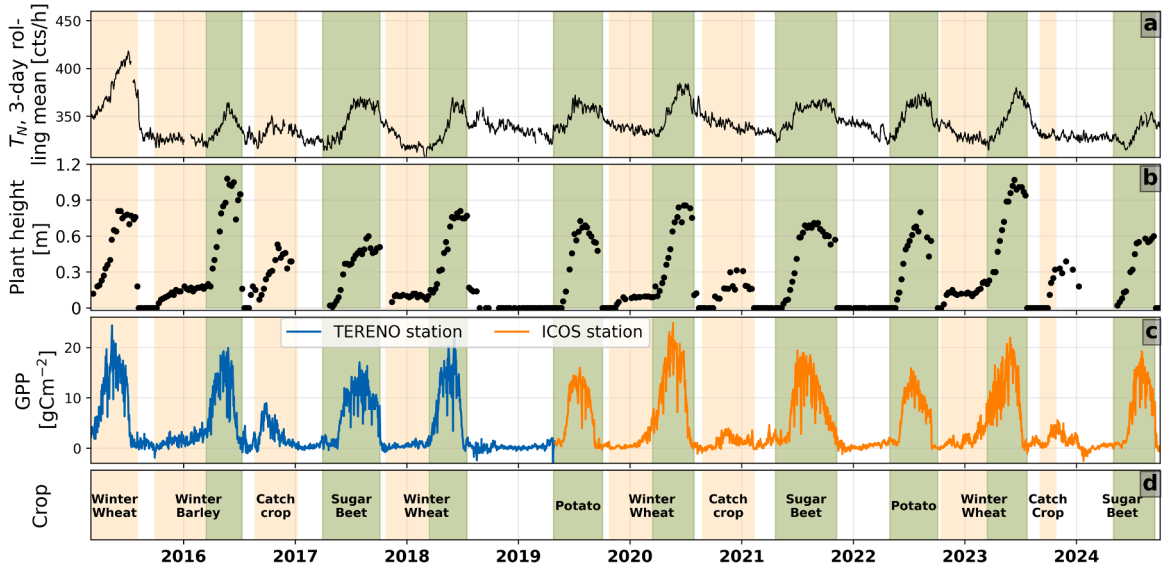

Fig. 4. Time series from the investigated site showing a) T_N, b) PH including the leftover stems of harvested plants measured in the vicinity of the ICOS station (see Fig. 2), c) GPP and f) crop rotation. The green areas indicate the periods investigated in this study, whereas the yellow areas indicate vegetated periods that were not included in the analysis.

patterns and seasonal variations: both increase rapidly at the start of vegetation growth, while values remain low during bare soil or catch crop periods. This suggests that T_N is responsive to plant growth and conditions. T_N seems to be mostly related to the long-term development of plants, while GPP can abruptly change due to changes in water availability or meteorological conditions. Thus, certain discrepancies between T_N and GPP must be expected. For example, GPP rises quickly at the beginning of the growing season, while T_N increases more gradually. In the case of sugar beet, GPP gradually decreases in the second half of the growing season. This is particularly the case in 2021 when sugar beet was harvested on 7th November, which is later in the growing season compared to 2017 and 2024 (5th October and 13th September, respectively) and thus is affected by less favourable growing conditions (e.g., lower temperature and solar radiation). In contrast, T_N remains rather constant during these growing periods of sugar beet, which is also the case for PH. For cereals (winter barley and winter wheat), GPP decreases rapidly after the onset of senescence towards the end of the growing season, while T_N shows a less pronounced decline. At the end of the potato growing season, desiccation practices lead to steep declines in GPP while T_N either remains rather stable (2019) or shows a decrease that is similar to that of GPP (2022). Senescence and desiccation are both characterized by significant water losses in plants. The slower decline of T_N compared to GPP could be related to factors such as additional hydrogen pools (e.g., below-ground biomass), plant structure, and the presence of elements with large neutron cross-sections in plants, such as boron. Finally, as T_N generally declines faster than PH, it can be expected that the relationship between T_N and PH may become less strong during these periods.

3.2. Thermal neutron intensity – plant height relationships

The all-crops T_N – *PH* relationship using manual PH measurements is shown in Fig. 5a-b. The T_N - SWC relationship is shown in Fig. 5c-d and uses SWC estimated from E_N (see Fig. 3d). Both relationships consider only the investigated growing seasons (green areas in Fig. 3) and the four investigated crops are shown with different colours. In Fig. 5a and 5c, T_N was normalized using the average T_N of the entire measurement period ($\overline{T_{N_a}}$), while in Fig. 5b and 5d, T_N was normalized with the average T_N of the first three days of each growing season ($\overline{T_N}$). A moderate positive correlation is apparent for T_N – *PH*, whereas T_N – *SWC* shows a weak negative correlation. Normalization with $\overline{T_{N_a}}$ resulted in an R^2 of 0.48 whereas normalization with $\overline{T_N}$ increased the R^2 to 0.66. Despite these promising R^2 values, the relationships with plant height show substantial scatter and seem to depend, at least in part, on the crop type. Thus, this scattering is likely due to differences in vegetation type and structure (Franz et al., 2013a; Jakobi et al., 2022). For T_N – *SWC*, R^2 values were substantially lower: 0.13 when using $\overline{T_{N_a}}$ and 0.09 when using $\overline{T_N}$. This weak T_N – *SWC* correlation may be related to a low sensitivity of thermal neutrons to SWC, but also, to the fact that the signal of bare detectors is also composed of a small portion of SWC-sensitive epithermal neutrons. Nonetheless, the stronger correlation of T_N – *PH* is apparent compared to that of T_N – *SWC*.

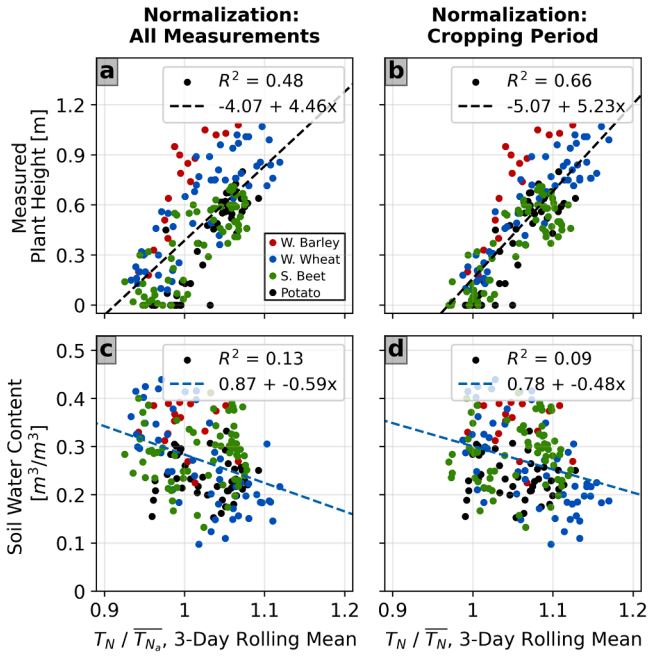

Fig. 5. Scatter plots showing PH (a-b) and SWC (c-d) as a function of T_N. Panels (a) and (c) use the mean of T_N during the entire study period ($\overline{T_{N_a}}$) while panels (b) and (d) use the mean of T_N during the first three days of the individual growing season ($\overline{T_N}$). In all panels, red points show winter barley, blue show winter wheat, wren show sugar beet, and black show potato. Corresponding linear regression models and R^2 are shown for each plot.

Fig. 6 shows scatter plots, linear regression models, and R^2 values of the crop-specific T_N – *PH* relationships. Here, T_N was normalized using the average T_N of the first three days of the growing season. The R^2 values for the crop-specific models were 0.84 for winter wheat (three growing seasons), 0.69 for sugar beet (three seasons), and 0.80 for potato (two seasons), which are all higher than the R^2 values of the all-crops model (Fig. 5b).

Table 1 shows the R^2 values and slopes of the T_N – *PH* relationships as well as the RMSE for predicting PH based on T_N (PH_{T_N}) for the annual linear regression models (with T_N normalized using the average T_N of the first three days of each growing season). The corresponding plots are shown in Appendix C (Fig. C1). In all annual models, the R^2 for the T_N – *PH* relationship is consistently higher than 0.72. Although the T_N – *PH* models all showed positive linear relationships, the slopes varied significantly. In the case of winter wheat, slope values were rather similar (between 4.52 and 5.14) while they were relatively low in sugar beet (3.63 to 5.08) and high in potato (5.69 and 8.71). The RMSE for predicting PH_{T_N} ranged from 0.07 m for the 2023 winter wheat to 0.15 m for the 2016 winter barley season. When expressed as a percentage of the maximum PH, the RMSE ranged from 9 % for the 2023 winter wheat season to 22 % for the 2024 sugar beet season.

Fig. 7 shows the model parameters from all the regression models with additional 95 % confidence intervals for all-crops and crop-specific models. For winter wheat, two annual models and the crop-specific model fall within the confidence interval of the all-crops model. The same applies to the crop-specific model of sugar beet and to one annual model for potato. The remaining models lie outside the uncertainty range of the all-crops model. These results suggest that T_N cannot be directly converted to PH with a single all-crops model for the investigated field, and that crop-specific or annual models are required.

3.3. PH, LAI, and dry AGB estimates from thermal neutrons

The results of the T_N-based estimates of PH (PH_{T_N}), LAI (LAI_{T_N}), and dry AGB (AGB_{T_N}) are shown in Fig. 8 and in Table 2, and are used to assess the ability of the CRNS to predict plant traits from T_N. Here, the crop-specific models of Fig. 6 were used to estimate PH from T_N (Fig. 8a), crop-specific relationships were used to estimate LAI (Fig. 8b), and annual relationships were used to estimate dry AGB (Fig. 8c). The PH_{T_N} estimates (green lines in Fig. 8b) generally agreed well with the manual PH measurements, with an RMSE of 0.13 m (12% of the maximum value), especially for winter wheat and winter barley. However, for sugar beet (both seasons) and potato (2019), the estimates tended to underestimate the manually measured values towards the second half of the growing season. A similar pattern can be observed when comparing PH_{T_N} with UAS-based PH measurements taken within a 45 m radius from the CRNS (red crosses in Fig. 8a, also see Fig. D1 in Appendix D). An exception is the 2022 potato season, where UAS-based

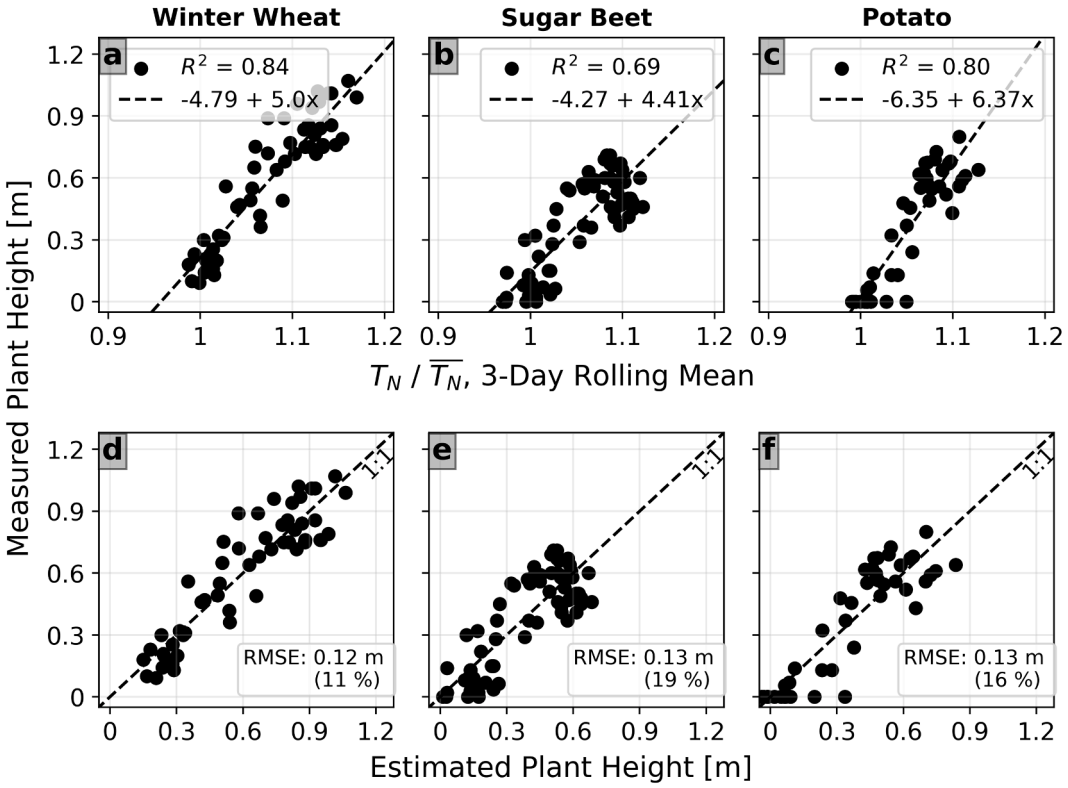

Fig. 6. Scatter plots with linear regression models and R^2 of PH as a function of T_N for a) winter wheat (3 seasons), b) sugar beet (3 seasons), and c) potato (2 seasons). 1:1 plots of measured and T_N-predicted PH are shown for d) winter wheat, e) sugar beet, and f) potato. In addition, the RMSE and the RMSE relative to the maximum PH in percent are given.

Table 1
Investigated crop, R^2, slope of the regression model, and RMSE of the annual T_N – PH relationships.

Year	2016	2017	2018	2019	2020	2021	2022	2023	2024
Crop	Winter Barley	Sugar Beet	Winter Wheat	Potato	Winter Wheat	Sugar Beet	Potato	Winter Wheat	Sugar Beet
R^2	0.72	0.85	0.89	0.87	0.89	0.84	0.89	0.90	0.75
Slope	7.28	3.63	4.52	8.71	5.03	6.28	5.69	5.14	5.08
RMSE (m)	0.15	0.07	0.08	0.10	0.09	0.11	0.09	0.10	0.11

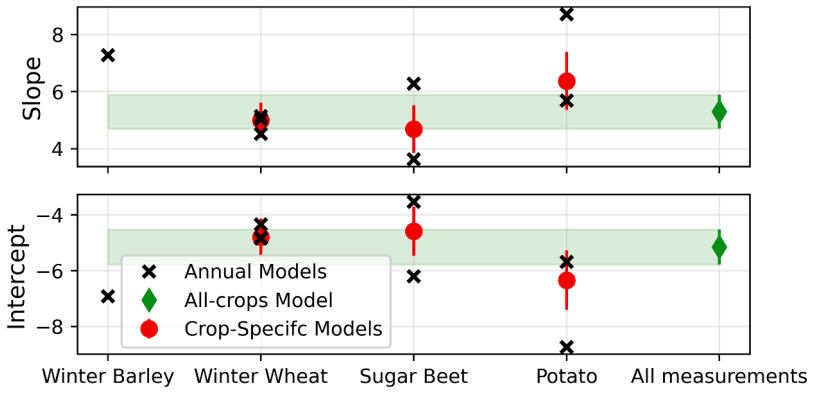

Fig. 7. Parameters of the thermal neutron intensity – plant height relationship models developed in this study. All-crops and crop-specific models are shown with the associated 95 % confidence intervals.

measurements are lower than both PH and PH_{T_N} by ~0.20-0.25 m. This discrepancy may be due to differences in the measurement methods: while PH was manually measured from the base to the top of the crop, UAS-based measurements sampled 25-60 points per 0.15 m, potentially underrepresenting the highest point of the canopy due its irregular shape (Montzka et al., 2023).

Table 2 shows the number of manual measurements, RMSE, and RMSE of the leave-one-out cross validation (LOOCV) of the crop-specific estimates. Overall, the LOOCV RMSE is only 3 to 12 % higher than the RMSE, which shows the good generalization and general reliability of the PH_{T_N} estimates.

Fig. 8c shows the LAI_{T_N} estimations (green lines) alongside the

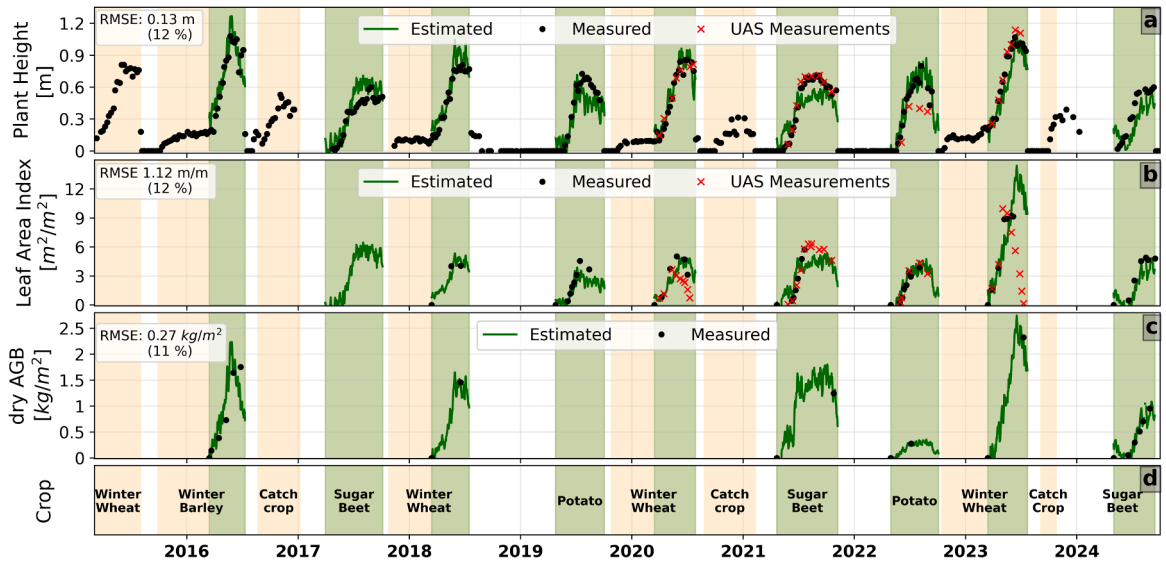

Fig. 8. Time series of manually measured (black dots), UAS-based (red crosses), and estimated values (green lines) for a) PH, b) LAI and GAI (UAS-based), and c) dry AGB. The RMSE and the RMSE relative to the maximal PH and LAI are also provided. Panel d) shows crop rotation. The green areas indicate the periods investigated in this study whereas the yellow areas indicate vegetated periods that not included in the analysis.

Table 2
Number of manual measurements, RMSE, and leave-one-out cross validation (LOOCV) RMSE of the crop-specific or annual estimates of PH, LAI, and dry AGB.

	Model or crop	N. of manual measurements	RMSE	LOOCV RMSE
PH (m)	Winter wheat	54	0.12	0.12
	Sugar beet	67	0.13	0.14
	Potato	43	0.13	0.13
	Winter barley	17	0.16	0.18
LAI (m^2/m^2)	Winter wheat (2018 and 2020)	7	1.08	1.70
	Winter wheat (2023)	6	1.37	1.86
	Potato	14	0.86	0.97
	Sugar beet	9	1.31	1.63
dry AGB (kg/m^2)	Winter barley (2016)	5	0.438	0.555
	Sugar beet (2024)	5	0.092	0.133

manual LAI measurements (black points). The RMSE for the investigated period was 1.12 (12 % of the maximum value). Overall, a visual inspection of Fig. 8c shows that LAI was well estimated except for winter wheat in 2023 where estimated values peak around 14 m^2/m^2, which is likely an unrealistic value for this crop. This overestimation is caused by two effects. First, the measured LAI values of 2023 are much higher (LAI mostly above 9) compared to previous growing seasons (LAI generally below 5), which is the result of exceptionally favourable growing conditions in the first half of 2023 (i.e., relatively high precipitation and SWC). Second, the high LAI values of manual measurements correspond to a time where T_N is still increasing. This suggests that, under certain environmental conditions, LAI measurements at the end of the growing season may be better suited to support LAI_T predictions. Fig. 8b also shows that LAI_{T_N} predictions matched well with UAS-based GAI for potato in 2022 and underestimated GAI for sugar beet in 2021 once a GAI of 4 is reached. In contrast, for winter wheat, UAS-based GAI values dropped below manually measured LAI values in the second half of the growing season due to the onset of senescence, highlighting how predictions based on T_N more accurately followed LAI than GAI during the study period. The crop-specific RMSE are shown in Table 2, together with the number of manual measurements and the LOOCV RMSE. For potato, the value of the LOOCV RMSE (0.97 m) is rather similar to the RMSE value (0.86 m). For the other three models, the LOOCV RMSE is from 24 to 57 % higher than the RMSE, most likely because of the low number of available manual measurements. Nonetheless, these results show the potential of estimating LAI from T_N.

For dry AGB (Fig. 8a), the number of validation measurements was limited due to the labour-intensive nature of destructive AGB measurements. Nevertheless, the results are promising, particularly for sugar beet in 2024 (RMSE of 0.092 kg/m^2, 10 % of maximum value) and winter barley in 2016 (RSME of 0.438 kg/m^2, 25 % of maximum value). Also, the LOOCV RMSE values shown in Table 2 are sufficiently similar to the RMSE, despite the relatively low number of manual measurements. By visually inspecting predictions in Fig. 8a, a noticeable difference in the estimated and measured dry AGB of sugar beet is apparent between 2021 and 2024. This discrepancy is likely related to the late seeding of sugar beet in 2024 compared to previous years. This was caused by the restricted access to the field due to unusually high soil wetness and resulted in a generally lower crop development compared to 2021 (i.e., lower measured PH, LAI, and dry AGB).

3.4. Potential of co-located CRNS and EC measurements

The results of this study showed that the CRNS provided SWC estimates that are likely more representative of the field-scale measured by the EC station compared to the point-scale sensors in the vicinity of EC station. Since both the CRNS and the nearby EC station measure over several hectares, these results suggest that the CRNS provides more comprehensive, convenient, and effective SWC estimates than point-scale sensors, making it ideal for long-term monitoring and for supporting EC measurements in agricultural settings. A visual comparison revealed a clear co-development of T_N measured by the CRNS and GPP estimated by the EC station, which highlights the potential of combined CRNS and GHG flux measurements.

The presented estimates of the vegetation properties, including PH, LAI, and dry AGB based on T_N measurements are also highly promising.

Despite certain limitations, especially when comparing crops grown under different climatic conditions (e.g., winter wheat in 2020 compared to 2023), PH, LAI, and dry AGB were estimated with sufficient precision, which could add significant value in multiple contexts. For example, a small number of manual dry AGB measurements could be integrated with measurements of T_N to provide continuous time series of dry AGB. Although it should be noted that the accuracy would most likely be lower compared to careful and extensive manual measurements, it is arguable that this disadvantage is outweighed by the relatively effortless nature of CRNS and by the fact that continuous data would provide significant added value in contexts such as long-term monitoring platforms and in the validation of land surface models or remote-sensing products.

3.5. Challenges and limitations

This study expands on previous research with a unique dataset covering a long-term investigation period, relatively stable environmental conditions, and extensive manual measurements for reference and validation. However, only a few dry AGB measurements were available due to the highly labour-intensive nature of such destructive measurements and the issues associated with removing large amounts of biomass from privately-owned agricultural fields. The long time series of almost ten years that was achieved in this study illustrates the need for correcting T_N for incoming cosmic radiation, as the 11-year solar cycle is clearly apparent in the pressure and humidity corrected $T_{N_{hp}}$. Also, during the 2015 winter wheat season, multiple CRNS with HDPE moderators led to unusually high thermal neutron intensities (Fig. B2c). This shows that high amounts of moderating material such as HDPE led to increased thermal neutron intensities recorded by bare detectors. This effect corresponds to what is observed with growing biomass, which supports the hypothesis of the dependence of the thermal neutron intensity on above-ground hydrogen pools.

This is the first study that investigates a 10-year long dataset of co-located CRNS, SWC, and vegetation properties at a single site. It showed that T_N and SWC dynamics do not consistently co-develop over this long period, with vegetation showing a dominant influence on T_N. Although a weak relationship was found for $T_N - SWC$, it can be argued that this may not be only related to the sensitivity of thermal neutrons to SWC but also to the small portion of epithermal neutrons measured by a bare detector. Future studies could further explore this topic or attempt to isolate a signal that is mostly composed of thermal neutrons, for example, by using a dual-spectra detector (Andreasen et al., 2016; Andreasen et al., 2023). Despite such considerations, the observed lower impact of SWC on T_N is apparent and may be due to atomic nuclei of plants limiting the penetration of thermal neutrons into the soil compared to what Jakobi et al. (2021) found for bare soil conditions. Furthermore, crop-specific relationships between measured T_N and PH were found, which suggests the influence of vegetation type and structure on measured thermal neutron intensity (Franz et al., 2013a; Jakobi et al., 2022). This would explain the scatter found in $T_N - PH$ relationships and thus stresses the need for specific crop and field calibrations. Additionally, PH, LAI, and dry AGB do not account for the large storage organs that sugar beet and potato develop below ground. In fact, below ground biomass may have an additional influence on T_N, which would explain the closer $T_N - PH$ relationship for winter wheat compared to sugar beet and potato. The physical reasons for differences in the strength of the correlations of T_N with plant traits depending on the plant type should be further investigated in future studies.

Finally, in the presented methodology, T_N was normalized by using the average values from 15th to 17th of March of each growing season ($\overline{T_N}$), and the average from 26th to 28th April for the year 2024. While the choice of these dates may seem arbitrary to a certain extent, they were suitable for the study area. Due to limited information, more objective selection methods could not be tested in this study, but future research could explore approaches such as the use of growing degree days from on-site meteorological stations or remote sensing information (Keramitsoglou et al., 2023).

3.6. Future perspectives

The thermal counter of the CRS-1000 used in this study has a relatively low count rate compared to some modern devices. Thus, on top of a daily aggregation, a 3-day smoothing was applied as this provided some improvements to PH, LAI, and dry AGB predictions, while the use of larger smoothing windows did not consistently provide additional benefits (not shown). Some modern detectors with higher count rates and efficiency could provide more accurate estimates and only require a daily aggregation due to the lower uncertainty of the measured neutron intensity. However, biomass changes occur at longer time scales, and the presented aggregation is deemed sufficient for most applications in agricultural environments. Moreover, other environmental conditions such as local altitude and geomagnetic cut-off rigidity can result in different count rates for the same instrument (Hertle et al., 2025; Zreda et al., 2012). It is thus possible that other ecosystems than agriculture or other geographic locations will require different integration strategies and further research is needed to address this topic.

The simultaneous and near-real time monitoring of SWC and plant development has great potential for both research and practical uses, and a CRNS can offer significant added value in long-term environmental observatories. For example, a CRNS can provide a more representative measurement of SWC, especially in agricultural environments where measurement consistency is hindered by frequent dismantling and reinstallation of point-scale sensors. Moreover, it could enable synergies with other measurements, such as EC measurements, due to their relatively similar footprint. Finally, CRNS data could aid in the development and validation of models that simulate the soil-vegetation-atmosphere continuum to study future agricultural and climatic scenarios (Arnault et al., 2024; Li et al., 2024). In future applications, biomass information derived from T_N could be used to correct E_N and improve the SWC estimates of the CRNS. However, the strength and validity of this method should be first tested in other contexts and ecosystems to obtain well founded and transferrable correction approaches. Finally, in agriculture, this approach could improve real-time management, such as in irrigation, by providing farmers with simultaneous estimates of SWC and crop development.

Overall, the promising results of this study suggest that the sensitivity of T_N measured with CRNS to plant traits deserves further investigation. Future studies should apply the presented relationships and, if necessary, recalibrate the models with local measurements. This should include additional crops, climatic conditions, agricultural practices, and different ecosystems such as grasslands, forests, and agroforestry. However, to increase the transferability of these methods, a particularly valuable avenue would be the use of neutron transport models such as the Ultra-Rapid Adaptable Neutron-Only Simulations model URANOS (Köhli et al., 2022). In fact, with CRNS, only the estimated energy range is known for a given detected neutron. Neutron transport models can simulate all the interactions that a neutron has with the environment (i.e., the soil-vegetation-atmosphere continuum) before it is detected, thus providing key information to interpret CRNS measurements. Currently, natural vegetation is represented in a rather simplified manner in neutron transport modelling (Brogi et al., 2023; Schrön et al., 2018) but more complex representations are under development (personal

communication with M. Köhli and J. Weimar). Moreover, the use of synthetic landscapes like the Virtual Joint Field Campaign by Francke et al. (2025) could help streamlining simulations and interpretations. This would result in a better understanding of CRNS measurements and their uncertainties for vegetation monitoring and would enhance the possibility to transfer the presented methods to other sites.

5. Conclusions

A cosmic-ray neutrons sensor (CRNS) provided long-term soil water content (SWC) estimates for an ICOS Class 1 ecosystem station (Selhausen, DE-RuS), which showed differences compared to the SWC estimated using a point-scale sensor network (RMSE of 0.063 m^3/m^3). Overall, the CRNS estimates were considered more representative of the field-scale area monitored by the nearby EC station than those of the sensor network.

A clear co-development of thermal neutron intensities (T_N) measured by the CRNS and gross primary productivity (GPP) estimated by the nearby EC station was observed. Specific differences between T_N and GPP dynamics that occurred during senescence and desiccation indicated that factors beyond plant water content can have an influence on T_N. It was also found that T_N is more closely related to changes in vegetation than changes in SWC. A good correlation between PH and T_N was found (e.g., R^2 between 0.69 and 0.84 for crop-specific models), and the difference between models showed that the relationship between PH and T_N may depend on vegetation structure.

T_N-based estimates of PH (PH_{T_N}) had a relatively good degree of accuracy (RMSE of 0.13 m). A leave-one-out cross validation (LOOCV) showed that LOOCV RMSE of the PH estimates were similar to their RMSE. Also estimates of LAI (LAI_{T_N}) and dry AGB (AGB_{T_N}) showed promising results (RMSE of 1.01 m^2/m^2 and 0.27 kg/m^2, respectively), although the difference between LOOCV RMSE and RMSE was higher than that of PH estimates.

The accuracy of plant traits predicted by the CRNS was lower compared to manual or destructive measurements. However, this can be outweighed by the effortless and continuous nature of CRNS measurements. Continuous and simultaneous estimates at relevant scales of SWC and plant traits using CRNS have significant potential, not only in long-term environmental monitoring platforms (e.g., Nasta et al. (2024), but also in other applications such as the validation of land surface models and remote-sensing products, as well as for applied decision-making processes in agriculture.

CRediT authorship contribution statement

C. Brogi: Writing – review & editing, Investigation, Methodology, Data curation, Visualization, Formal analysis, Writing – original draft, Conceptualization. **J. Jakobi:** Writing – review & editing, Investigation, Visualization, Conceptualization, Formal analysis, Writing – original draft, Methodology, Data curation. **J.A. Huisman:** Conceptualization, Writing – review & editing, Methodology. **M. Schmidt:** Data curation, Methodology, Writing – review & editing. **C. Montzka:** Writing – review & editing, Data curation, Methodology. **J.S. Bates:** Writing – review & editing, Methodology, Data curation. **S. Akter:** Writing – review & editing, Data curation. **H.R. Bogena:** Methodology, Conceptualization, Writing – review & editing.

Declaration of competing interest

The authors declare that they have no known competing financial interests or personal relationships that could have appeared to influence the work reported in this paper.

Acknowledgements

The authors thank Nicole Adels, Shirin Bagheri, Daniel Dolfus, Odilia Esser, Hannah Fuchs, Martina Kettler, Sirgit Kummer, Bernd Schilling, and Ansgar Weuthen for the support in instrument installation and maintenance, and with soil and crop measurements and sample processing. We also thank the ICOS ETC team at Forschungszentrum Jülich (Alexander Graf, Nils Becker, and Andreas Haustein) for their work in operating the Selhausen station and for providing detailed and refined data products, which significantly contributed to our research. Support was received from the Deutsche Forschungsgemeinschaft (DFG, German Research Foundation) project 357874777 of the research unit FOR 2694 Cosmic Sense, from the WASCAL/CONCERT project 01LG2089Ch financed by the Federal Ministry of Education and Research, from SFB-TR32 Patterns in Soil-Vegetation-Atmosphere Systems: Monitoring, Modelling and Data Assimilation funded by the Deutsche Forschungsgemeinschaft (DFG), from TERENO (TERrestrial Environmental Observatories), from MOSES (Modular Observation Solutions for Earth Systems) funded by the Helmholtz-Gemeinschaft, and from the Deutsche Forschungsgemeinschaft (DFG, German Research Foundation) under Germany's Excellence Strategy-EXC 2070-390732324 and - SFB1502/1-2022 - Project number: 450058266 (collaborative research centre DETECT). Finally, the NMDB database funded by EU-FP7 is also acknowledged.

Appendix A

The humidity correction (Eq. 5) was originally developed to correct the influence of humidity on epithermal neutrons. Recent findings by Rasche et al. (2023) suggest that Eq. 5 should be modified for the correction of thermal neutrons to avoid overcorrection. They proposed the following modified correction:

$$f_{ht} = 1 + 0.0021(h - h_o) \tag{A1}$$

where h is the measured absolute air humidity [g/cm^3], and h_o [g/cm^3] is the average air humidity over the investigation period, and f_{ht} is the correction factor to be used in Equation 6 for the correction of thermal neutrons. Fig. A1 shows the thermal neutron intensity (T_N) for the monitored period corrected by using either the approach of Rosolem et al. (2013) or that of Rasche et al. (2023). The use of Eq. (A1) results in certain differences but, overall, the dynamics appear to be rather similar to those obtained with Eq. (5) and a more in-depth analysis would be needed to better evaluate the advantages of each method. Overall, the impact of replacing Eq. (5) with Eq. (A1) on the $T_N - PH$ relationships was rather limited. For the annual models, the changes in R^2 ranged from +0.01 to -0.11 (average change of 0.03). The impact of using either correction method is probably reduced by the use a 3-day rolling mean smoothing approach on top of the daily aggregation of thermal neutron intensity.

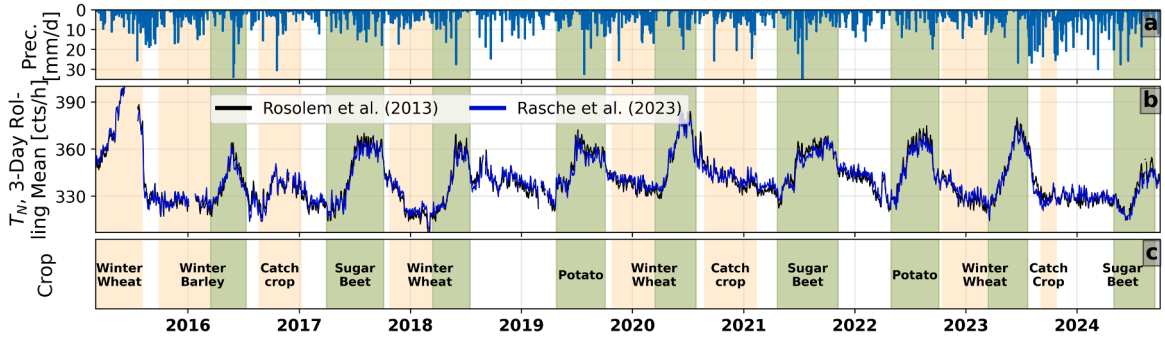

Fig. A1. Time series from the investigated site showing a) precipitation and b) T_N with, in black, humidity correction from Rosolem et al. (2013) and, in blue, humidity correction from Rasche et al. (2023). In c), the green areas indicate the periods investigated in this study whereas yellow areas indicate vegetated periods that were not included in the analysis.

Appendix B

Fig. B1 shows the experimental site and the position of the instrumentation. In particular, Fig. B1c shows the temporary installation of multiple CRNS that were in place until the end of the 2015 winter wheat growing season. More information on this installation is provided in Fuchs (2016) and Jakobi et al. (2022).

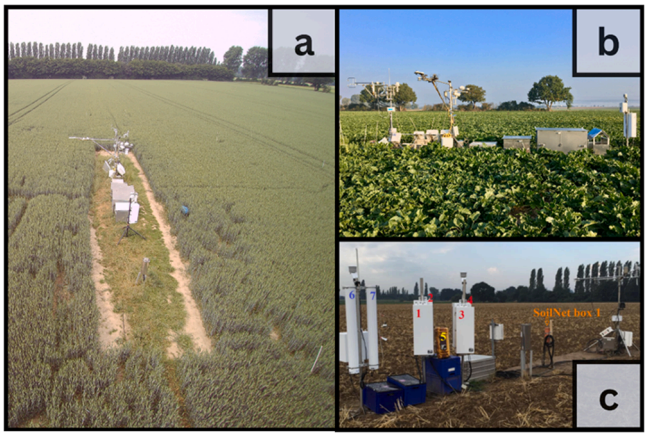

Fig. B1. Pictures from the experimental site, a) UAS imagery, b) setup as for most of the investigation period, and c) setup of multiple CRNS as during the 2015 winter wheat growing season (photo by: H. Fuchs).

Fig. B2 shows a comparison of the $T_N - PH$ relationship between the 2015 winter wheat season and the remaining winter wheat seasons (Fig. B2a) and between 2015 and the entire investigated period (Fig. B2b). The differences for the 2015 season are apparent, and were attributed to high thermal neutron counts due to closely spaced detectors with HDPE moderators (Fig. B1c).

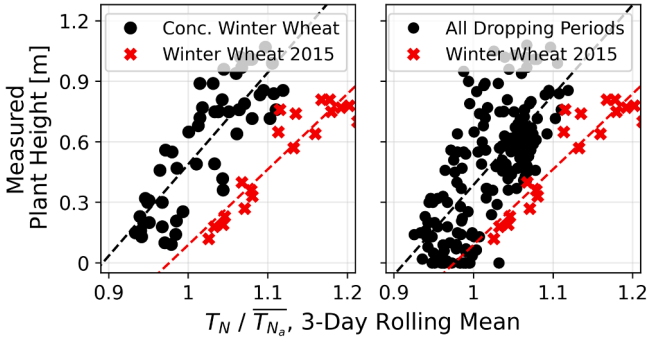

Fig. B2. Scatter plots showing plant height as functions of thermal neutron intensity for the 2015 winter wheat season (red in panels a and b) and for a) the 2018, 2020, and 2023 winter wheat seasons or for b) all the 2016-2023 growing seasons (both black).

Appendix C

Fig. C1 shows the yearly T_N – PH relationships with associated R^2 and slope of the regression models that are summarized in Table 1. Additionally, Fig. C2 shows the yearly relationships between manually measured PH and predicted PH_{T_N} including RMSE (as indicated in Table 1) and RMSE relative to the maximum measured PH.

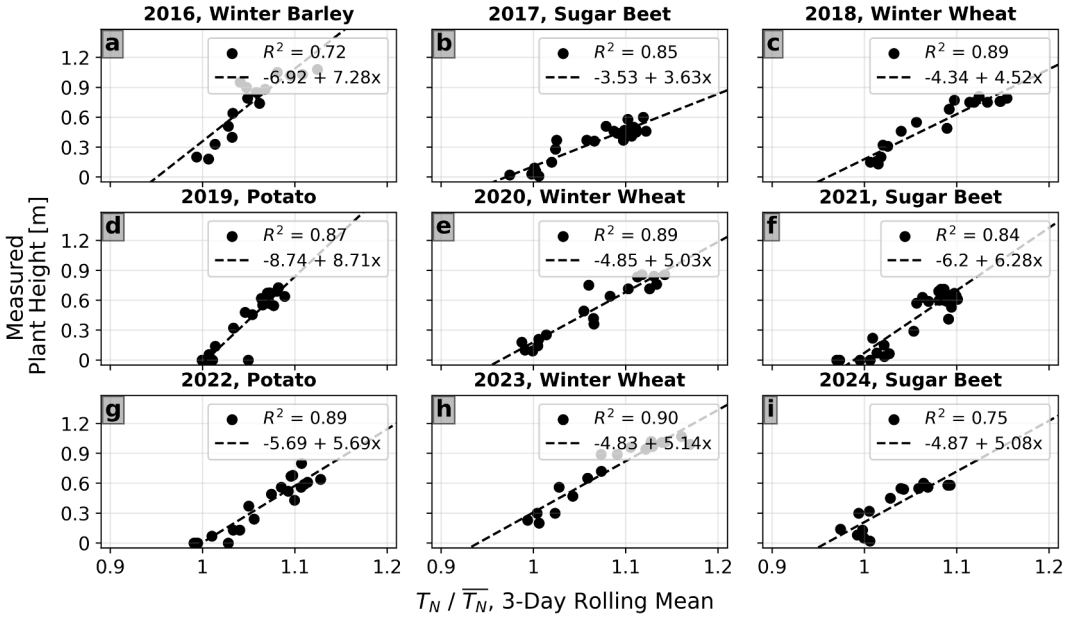

Fig. C1. Annual plant height (PH) as a function of thermal neutron intensity (T_N). Corresponding linear regression models and R^2 are shown for each plot.

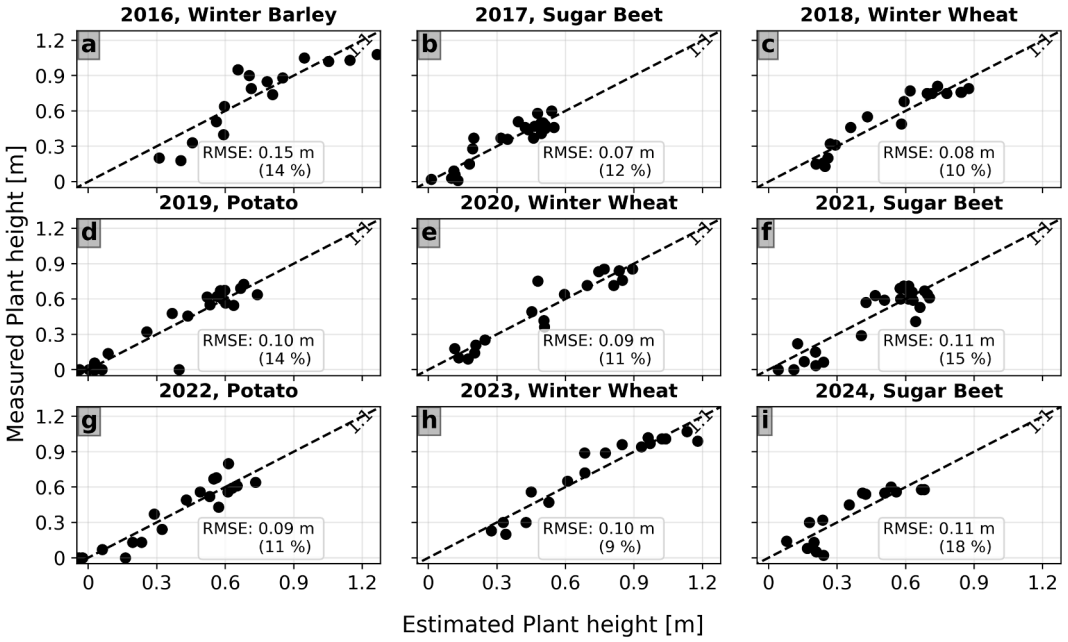

Fig. C2. Scatter plots of measured and T_N-predicted PH with the RMSE and the RMSE relative to the maximum PH in percent.

Appendix D

Fig. D1 shows UAS-based PH (left panel) and GAI measurements (right panel) in the investigated field for the 13th of August 2021.

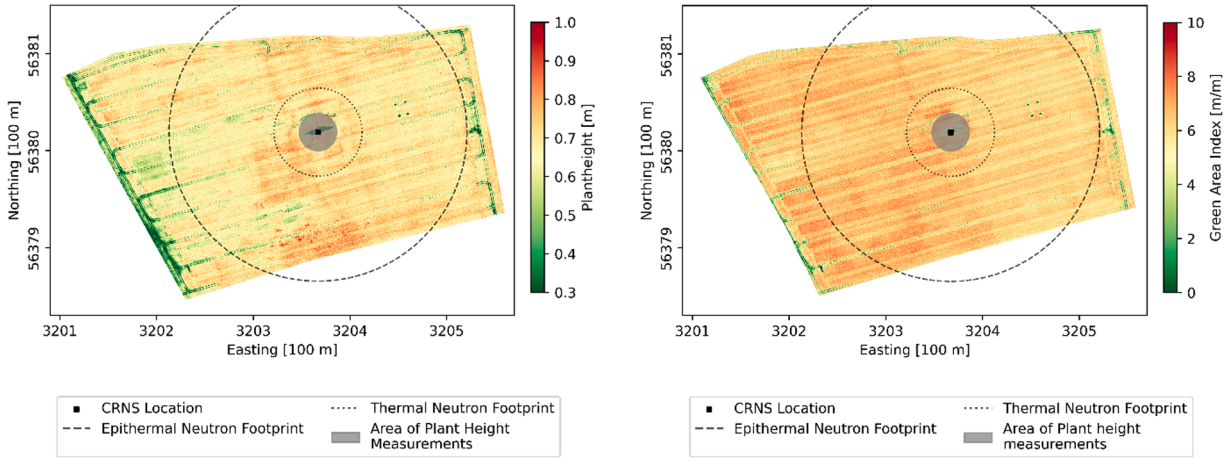

Fig. D1. Study area with UAS-based PH (left panel) and GAI (right panel) measured on the 13th of August 2021. In addition, the locations of the cosmic ray neutron sensor (CRNS), and the epithermal and thermal neutron footprint radii are shown (i.e., 154 m and 45 m, respectively).

Data availability

The datasets and codes used in this study can be downloaded at: https://github.com/CosimoBrogi/Data_plots_AGRFORMET-D-25-00237R1/releases/tag/AGRFORMET-D-25-00237R1.

References

Al-Mashharawi, S.K., Steele-Dunne, S.C., El Hajj, M.M., Schrön, M., Doussan, C., Courault, D., Franz, T.E., McCabe, M.F., 2025. Accounting for biomass water equivalent variations in soil moisture retrievals from cosmic ray neutron sensor. Agric. Water. Manage 313, 109493.

Ali, M., Montzka, C., Stadler, A., Menz, G., Thonfeld, F., Vereecken, H., 2015. Estimation and validation of RapidEye-based time-series of leaf area index for winter wheat in the Rur catchment (Germany). Remote Sens (Basel) 7 (3), 2808–2831.

Andreasen, M., Jensen, K.H., Desilets, D., Franz, T.E., Zreda, M., Bogena, H.R., Looms, M. C., 2017. Status and perspectives on the cosmic-ray neutron method for soil moisture estimation and other environmental science applications. Vadose Zone Journal 16 (8), 1–11.

Andreasen, M., Jensen, K.H., Zreda, M., Desilets, D., Bogena, H., Looms, M.C., 2016. Modeling cosmic ray neutron field measurements. Water Resour Res 52 (8), 6451–6471.

Andreasen, M., Kragh, S.J., Meyer, R., Jensen, K.H., Looms, M.C., 2023. Mapping spatiotemporal soil moisture in highly heterogeneous agricultural landscapes using mobile dual-spectra cosmic-ray neutron sensing. Vadose Zone Journal, e20287.

Aranguren, M., Castellón, A., Aizpurua, A., 2020. Crop sensor based non-destructive estimation of nitrogen nutritional status, yield, and grain protein content in wheat. Agriculture 10 (5), 148.

Arnault, J., Benjamin, F., Schrön, M., Bogena, H.R., Hendricks Franssen, H.J., Kinstmann, H., 2024. Role of infiltration on land–atmosphere feedbacks in Central Europe: fully coupled WRF-Hydro simulations evaluated with cosmic-ray neutron soil moisture measurements. Journal of Hydrometeorology Accepted for publication.

Baatz, R., Bogena, H.R., Hendricks Franssen, H.-J., Huisman, J.A., Montzka, C., Vereecken, H., 2015. An empirical vegetation correction for soil water content quantification using cosmic ray probes. Water Resour Res 51 (4), 2030–2046.

Baatz, R., Hendricks Franssen, H.-J., Han, X., Hoar, T., Bogena, H.R., Vereecken, H., 2017. Evaluating the value of a network of cosmic-ray probes for improving land surface modeling. Hydrol. Earth. Syst. Sci. 21, 2509–2530.

Babaeian, E., Sadeghi, M., Franz, T.E., Jones, S., Tuller, M., 2018. Mapping soil moisture with the OPtical TRApezoid Model (OPTRAM) based on long-term MODIS observations. Remote Sens Environ 211, 425–440.

Balasubrahmanyan, V.K., 1969. Solar activity and the 11-year modulation of cosmic rays. Sol Phys 7 (1), 39–45.

Baret, F., Houles, V., Guérif, M., 2007. Quantification of plant stress using remote sensing observations and crop models: the case of nitrogen management. J. Exp. Bot. 58 (4), 869–880.

Baroni, G., Oswald, S., 2015. A scaling approach for the assessment of biomass changes and rainfall interception using cosmic-ray neutron sensing. J Hydrol 525, 264–276.

Bates, J.S., Montzka, C., Schmidt, M., Jonard, F., 2021. Estimating canopy density parameters time-series for winter wheat using UAS mounted LiDAR. Remote Sens (Basel) 13 (4), 710.

Beillouin, D., Schauberger, B., Bastos, A., Ciais, P., Makowski, D., 2020. Impact of extreme weather conditions on European crop production in 2018. Philosophical Transactions of the Royal Society B 375 (1810), 20190510.

Biernacki, M., Bruton, B.D., 2000. Comparison of leaf-area index with root weight for assessing plant damage by soil-borne pathogens. VII Eucarpia Meeting on Cucurbit Genetics and Breeding 510, 163–170.

Boas, T., Bogena, H., Grünwald, T., Heinesch, B., Ryu, D., Schmidt, M., Vereecken, H., Western, A., Hendricks Franssen, H.-J., 2021. Improving the representation of cropland sites in the Community Land Model (CLM) version 5.0. Geosci. Model. Dev. 14 (1), 573–601.

Bogena, H., Huisman, J., Schilling, B., Weuthen, A., Vereecken, H., 2017. Effective calibration of low-cost soil water content sensors. Sensors 17 (1), 208.

Bogena, H., Schrön, M., Jakobi, J., Ney, P., Zacharias, S., Andreasen, M., Baatz, R., Boorman, D., Duygu, B.M., Eguibar-Galán, M.A., 2022a. COSMOS-Europe: A European network of cosmic-ray neutron soil moisture sensors. Earth System Science Data Discussions 1–33.

Bogena, H.R., Herbst, M., Huisman, J.A., Rosenbaum, U., Weuthen, A., Vereecken, H., 2010. Potential of wireless sensor networks for measuring soil water content variability. Vadose Zone Journal 9 (4), 1002–1013.

Bogena, H.R., Herrmann, F., Jakobi, J., Brogi, C., Ilias, A., Huisman, J.A., Panagopoulos, A., Pisinaras, V., 2020. Monitoring of snowpack dynamics with cosmic-ray neutron probes: A comparison of four conversion methods. Front. Water. 2, 19.

Bogena, H.R., Montzka, C., Huisman, J.A., Graf, A., Schmidt, M., Stockinger, M., von Hebel, C., Hendricks-Franssen, H.J., van der Kruk, J., Tappe, W., 2018. The TERENO-Rur Hydrological observatory: A multiscale multi-compartment research platform for the advancement of hydrological science. Vadose Zone Journal 17 (1).

Bogena, H.R., Weuthen, A., Huisman, J.A., 2022b. Recent developments in wireless soil moisture sensing to support scientific research and agricultural management. Sensors 22 (24), 9792.

Bréda, N.J., 2003. Ground-based measurements of leaf area index: a review of methods, instruments and current controversies. J. Exp. Bot. 54 (392), 2403–2417.

Brogi, C., Huisman, J.A., Herbst, M., Weihermüller, L., Klosterhalfen, A., Montzka, C., Reichenau, T.G., Vereecken, H., 2020. Simulation of spatial variability in crop LAI and yield using agro-ecosystem modelling and geophysics-based quantitative soil information. Vadose Zone Journal.

Brogi, C., Huisman, J.A., Pätzold, S., von Hebel, C., Weihermüller, L., Kaufmann, M.S., van der Kruk, J., Vereecken, H., 2019. Large-scale soil mapping using multi-configuration EMI and supervised image classification. Geoderma 335, 133–148.

Brogi, C., Huisman, J.A., Weihermüller, L., Herbst, M., Vereecken, H., 2021. Added value of geophysics-based soil mapping in agro-ecosystem simulations. Soil 7 (1), 125–143.

Brogi, C., Pisinaras, V., Köhli, M., Dombrowski, O., Hendricks Franssen, H., Babakos, K., Chatzi, A., Panagopoulos, A., Bogena, H., 2023. Monitoring irrigation in small orchards with cosmic-ray neutron sensors. Sensors 23 (5), 2378.

Catchpole, W., Wheeler, C., 1992. Estimating plant biomass: a review of techniques. Australian Journal of Ecology 17 (2), 121–131.

Condon, A.G., 2020. Drying times: plant traits to improve crop water use efficiency and yield. J. Exp. Bot. 71 (7), 2239–2252.

Coopersmith, E.J., Cosh, M.H., Daughtry, C.S., 2014. Field-scale moisture estimates using COSMOS sensors: A validation study with temporary networks and leaf-area-indices. J Hydrol 519, 637–643.

Desilets, D., Zreda, M., 2001. On scaling cosmogenic nuclide production rates for altitude and latitude using cosmic-ray measurements. Earth Planet. Sci. Lett. 193 (1-2), 213–225.
Desilets, D., Zreda, M., 2003. Spatial and temporal distribution of secondary cosmic-ray nucleon intensities and applications to in situ cosmogenic dating. Earth Planet. Sci. Lett. 206 (1-2), 21–42.
Desilets, D., Zreda, M., Ferré, T.P.A., 2010. Nature's neutron probe: land surface hydrology at an elusive scale with cosmic rays. Water Resour Res 46 (11).
ESRI, 2024. DIgitalGlobe, GeoEye, Earthstar Geographics, CNES/Airbus DS, USDA, AEX, Getmapping, Aerogrid, IGN, IGP, swisstopo, and the GIS User Comunity.
Fang, H., Baret, F., Plummer, S., Schaepman-Strub, G., 2019. An overview of global leaf area index (LAI): methods, products, validation, and applications. Reviews of Geophysics 57 (3), 739–799.
Finkenbiner, C.E., Franz, T.E., Gibson, J., Heeren, D.M., Luck, J., 2019. Integration of hydrogeophysical datasets and empirical orthogonal functions for improved irrigation water management. Precis. Agric. 20 (1), 78–100.
Foley, J.A., Ramankutty, N., Brauman, K.A., Cassidy, E.S., Gerber, J.S., Johnston, M., Mueller, N.D., O'Connell, C., Ray, D.K., West, P.C., 2011. Solutions for a cultivated planet. Nature 478 (7369), 337.
Francke, T., Brogi, C., Duarte Rocha, A., Förster, M., Heistermann, M., Köhli, M., Rasche, D., Reich, M., Schattan, P., Scheiffele, L., Schrön, M., 2025. Virtual Joint Field Campaign: a framework of synthetic landscapes to assess multiscale measurement methods of water storage. Geosci. Model. Dev. 18 (3), 819–842.
Franz, T., Wahbi, A., Vreugdenhil, M., Weltin, G., Heng, L., Oismueller, M., Strauss, P., Dercon, G., Desilets, D., 2016. Using cosmic-ray neutron probes to monitor landscape scale soil water content in mixed land use agricultural systems. Appl. Environ. Soil. Sci. 2016.
Franz, T.E., Zreda, M., Ferre, T., Rosolem, R., 2013a. An assessment of the effect of horizontal soil moisture heterogeneity on the area-average measurement of cosmic-ray neutrons. Water Resour Res 49 (10), 6450–6458.
Franz, T.E., Zreda, M., Rosolem, R., Hornbuckle, B.K., Irvin, S.L., Adams, H., Kolb, T.E., Zweck, C., Shuttleworth, W.J., 2013b. Ecosystem-scale measurements of biomass water using cosmic ray neutrons. Geophys Res Lett 40 (15), 3929–3933.
Friedli, M., Kirchgessner, N., Grieder, C., Liebisch, F., Mannale, M., Walter, A., 2016. Terrestrial 3D laser scanning to track the increase in canopy height of both monocot and dicot crop species under field conditions. Plant Methods 12, 1–15.
Fuchs, H., 2016. Effects of biomass on soil moisture measurements using cosmic-ray neutron probes. University of Duisburg-Essen, IBG-3 Agrosphere Institute, Forschungszentrum Jülich.
Graf, A., Klosterhalfen, A., Arriga, N., Bernhofer, C., Bogena, H., Bornet, F., Brüggemann, N., Brümmer, C., Buchmann, N., Chi, J., 2020. Altered energy partitioning across terrestrial ecosystems in the European drought year 2018. Philosophical Transactions of the Royal Society B 375 (1810), 20190524.
Gugerli, R., Salzmann, N., Huss, M., Desilets, D., 2019. Continuous and autonomous snow water equivalent measurements by a cosmic ray sensor on an alpine glacier. Cryosphere 13 (12), 3413–3434.
Hao, S., Ryu, D., Western, A.W., Perry, E., Bogena, H., Franssen, H.J.H., 2024. Global sensitivity analysis of APSIM-wheat yield predictions to model parameters and inputs. Ecol Modell 487, 110551.
Hawdon, A., McJannet, D., Wallace, J., 2014. Calibration and correction procedures for cosmic-ray neutron soil moisture probes located across Australia. Water Resour Res 50 (6), 5029–5043.
Hertle, L., Zacharias, S., Larsen, N., Rasche, D., Schrön, M., 2025. Neutron monitor based incoming flux correction for cosmic-ray Neutron sensing of soil moisture. Authorea Preprints.
Jakobi, J., Huisman, J., Vereecken, H., Diekkrüger, B., Bogena, H., 2018. Cosmic ray neutron sensing for simultaneous soil water content and biomass quantification in drought conditions. Water Resour Res 54 (10), 7383–7402.
Jakobi, J., Huisman, J.A., Fuchs, H., Vereecken, H., Bogena, H.R.. Potential of thermal neutrons to correct cosmic-ray neutron soil moisture content measurements for dynamic biomass effects. https://agupubs.onlinelibrary.wiley.com/doi/full/10.1029/2022WR031972.
Jakobi, J., Huisman, J.A., Köhli, M., Rasche, D., Vereecken, H., Bogena, H.R., 2021. The footprint characteristics of cosmic ray thermal neutrons. Geophys Res Lett 48 (15), e2021GL094281.
Jakobi, J., Huisman, J.H., Schrön, M., Fiedler, J., Brogi, C., Vereecken, H., Bogena, H.R., 2020. Error estimation for soil moisture measurements with cosmic-ray neutron sensing and implications for rover surveys. Front. Water.
Jiang, Y., Li, C., Paterson, A.H., 2016. High throughput phenotyping of cotton plant height using depth images under field conditions. Comput. Electron. Agric. 130, 57–68.
Jonckheere, I., Fleck, S., Nackaerts, K., Muys, B., Coppin, P., Weiss, M., Baret, F., 2004. Review of methods for in situ leaf area index determination: part I. Theories, sensors and hemispherical photography. Agric For Meteorol 121 (1-2), 19–35.
Keramitsoglou, I., Sismanidis, P., Sykioti, O., Pisinaras, V., Tsakmakis, I., Panagopoulos, A., Argyriou, A., Kiranoudis, C.T., 2023. SENSE-GDD: A satellite-derived temperature monitoring service to provide growing degree days. Agriculture 13 (5), 1108.
Knoll, G.F., 2010. Radiation detection and measurement, 4th ed., xxvi. John Wiley, Hoboken N.J, p. 830.
Köhli, M., Schrön, M., Zacharias, S., Schmidt, U., 2022. URANOS v1.0 - the Ultra Rapid adaptable neutron-only simulation for environmental research. Geosci. Model Dev. Discuss. 2022, 1–48.
Köhli, M., Schrön, M., Zreda, M., Schmidt, U., Dietrich, P., Zacharias, S., 2015. Footprint characteristics revised for field-scale soil moisture monitoring with cosmic-ray neutrons. Water Resour Res 51 (7), 5772–5790.
Korres, W., Reichenau, T., Fiener, P., Koyama, C., Bogena, H.R., Cornelissen, T., Baatz, R., Herbst, M., Diekkrüger, B., Vereecken, H., 2015. Spatio-temporal soil moisture patterns–A meta-analysis using plot to catchment scale data. J Hydrol 520, 326–341.
Li, D., Schrön, M., Kohli, M., Bogena, H.R., Weimar, J., Jiménez Bello, M.A., Han, X., Martínez-Gimeno, M.A., Zacharias, S., Vereecken, H., Hendricks Franssen, H.J., 2019. Can drip irrigation be scheduled with cosmic-ray neutron sensing? Vadose zone journal 18 (1), 1–13.
Li, F., Bogena, H.R., Bayat, B., Kurtz, W., Hendricks Franssen, H.J., 2024. Can a sparse network of cosmic ray neutron sensors improve soil moisture and evapotranspiration estimation at the larger catchment scale? Water Resour Res 60 (1) e2023WR035056.
Majone, B., Viani, F., Filippi, E., Bellin, A., Massa, A., Toller, G., Robol, F., Salucci, M., 2013. Wireless sensor network deployment for monitoring soil moisture dynamics at the field scale. Procedia Environ Sci 19, 426–435.
Marshall, M., Thenkabail, P., 2015. Developing in situ non-destructive estimates of crop biomass to address issues of scale in remote sensing. Remote Sens (Basel) 7 (1), 808–835.
Mauder, M., Cuntz, M., Drüe, C., Graf, A., Rebmann, C., Schmid, H.P., Schmidt, M., Steinbrecher, R., 2013. A strategy for quality and uncertainty assessment of long-term eddy-covariance measurements. Agric For Meteorol 169, 122–135.
Mauder, M., Foken, T., 2015. Documentation and instruction manual of the eddy-covariance software package TK3 (update). https://epub.uni-bayreuth.de/id/eprint/342/1/ARBERG046.pdf.
McJannet, D., Desilets, D., 2023. Incoming neutron flux corrections for cosmic-ray soil and snow sensors using the global neutron monitor network. Water Resour Res 59 (4) e2022WR033889.
McJannet, D., Franz, T., Hawdon, A., Boadle, D., Baker, B., Almeida, A., Silberstein, R., Lambert, T., Desilets, D., 2014. Field testing of the universal calibration function for determination of soil moisture with cosmic-ray neutrons. Water Resour Res 50 (6), 5235–5248.
McJannet, D., Hawdon, A., Baker, B., Renzullo, L., Searle, R., 2017. Multiscale soil moisture estimates using static and roving cosmic-ray soil moisture sensors. Hydrol. Earth. Syst. Sci. 21 (12), 6049–6067.
Mohanty, B.P., Cosh, M.H., Lakshmi, V., Montzka, C., 2017. Soil moisture remote sensing: State-of-the-science. Vadose Zone Journal 16 (1), 1–9.
Montzka, C., Bogena, H.R., Zreda, M., Monerris, A., Morrison, R., Muddu, S., Vereecken, H., 2017. Validation of spaceborne and modelled surface soil moisture products with cosmic-ray neutron probes. Remote Sens (Basel) 9 (2), 103.
Montzka, C., Donat, M., Raj, R., Welter, P., Bates, J.S., 2023. Sensitivity of LiDAR parameters to aboveground biomass in winter spelt. Drones 7 (2), 121.
Nasta, P., Blöschl, G., Bogena, H.R., Zacharias, S., Baatz, R., De Lannoy, G., Jensen, K.H., Manfreda, S., Pfister, L., Tarquis, A.M., van Meerveld, I., Voltz, M., Zeng, Y., Kustas, W., Li, X., Vereecken, H., Romano, N., 2024. HESS opinions: towards a common vision for the future of hydrological observatories. EGUsphere 2024, 1–20.
Ohnemus, T., Zacharias, S., Dirnböck, T., Bäck, J., Brack, W., Forsius, M., Mallast, U., Nikolaidis, N.P., Peterseil, J., Piscart, C., 2024. The eLTER research infrastructure: current design and coverage of environmental and socio-ecological gradients. Environmental and Sustainability Indicators 23, 100456.
Pastorello, G., Trotta, C., Canfora, E., Chu, H., Christianson, D., Cheah, Y.-W., Poindexter, C., Chen, J., Elbashandy, A., Humphrey, M., Isaac, P., Polidori, D., Reichstein, M., Ribeca, A., van Ingen, C., Vuichard, N., Zhang, L., Amiro, B., Ammann, C., Arain, M.A., Ardö, J., Arkebauer, T., Arndt, S.K., Arriga, N., Aubinet, M., Aurela, M., Baldocchi, D., Barr, A., Beamesderfer, E., Marchesini, L.B., Bergeron, O., Beringer, J., Bernhofer, C., Berveiller, D., Billesbach, D., Black, T.A., Blanken, P.D., Bohrer, G., Boike, J., Bolstad, P.V., Bonal, D., Bonnefond, J.-M., Bowling, D.R., Bracho, R., Brodeur, J., Brümmer, C., Buchmann, N., Burban, B., Burns, S.P., Buysse, P., Cale, P., Cavagna, M., Cellier, P., Chen, S., Chini, I., Christensen, T.R., Cleverly, J., Collalti, A., Consalvo, C., Cook, B.D., Cook, D., Coursolle, C., Cremonese, E., Curtis, P.S., D'Andrea, E., da Rocha, H., Dai, X., Davis, K.J., Cinti, B.D., Grandcourt, A.d., Ligne, A.D., De Oliveira, R.C., Delpierre, N., Desai, A.R., Di Bella, C.M., Tommasi, P.d., Dolman, H., Domingo, F., Dong, G., Dore, S., Duce, P., Dufrêne, E., Dunn, A., Dušek, J., Eamus, D., Eichelmann, U., ElKhidir, H.A.M., Eugster, W., Ewenz, C.M., Ewers, B., Famulari, D., Fares, S., Feigenwinter, I., Feitz, A., Fensholt, R., Filippa, G., Fischer, M., Frank, J., Galvagno, M., Gharun, M., Gianelle, D., Gielen, B., Gioli, B., Gitelson, A., Goded, I., Goeckede, M., Goldstein, A.H., Gough, C.M., Goulden, M.L., Graf, A., Griebel, A., Gruening, C., Grünwald, T., Hammerle, A., Han, S., Han, X., Hansen, B.U., Hanson, C., Hatakka, J., He, Y., Hehn, M., Heinesch, B., Hinko-Najera, N., Hörtnagl, L., Hutley, L., Ibrom, A., Ikawa, H., Jackowicz-Korczynski, M., Janouš, D., Jans, W., Jassal, R., Jiang, S., Kato, T., Khomik, M., Klatt, J., Knohl, A., Knox, S., Kobayashi, H., Koerber, G., Kolle, O., Kosugi, Y., Kotani, A., Kowalski, A., Kruijt, B., Kurbatova, J., Kutsch, W.L., Kwon, H., Launiainen, S., Laurila, T., Law, B., Leuning, R., Li, Y., Liddell, M., Limousin, J.-M., Lion, M., Liska, A.J., Lohila, A., López-Ballesteros, A., López-Blanco, E., Loubet, B., Loustau, D., Lucas-Moffat, A., Lüers, J., Ma, S., Macfarlane, C., Magliulo, V., Maier, R., Mammarella, I., Manca, G., Marcolla, B., Margolis, H.A., Marras, S., Massman, W., Mastepanov, M., Matamala, R., Matthes, J.H., Mazzenga, F., McCaughey, H., McHugh, I., McMillan, A.M.S., Merbold, L., Meyer, W., Meyers, T., Miller, S.D., Minerbi, S., Moderow, U., Monson, R.K., Montagnani, L., Moore, C.E., Moors, E., Moreaux, V., Moureaux, C., Munger, J.W., Nakai, T., Neirynck, J., Nesic, Z., Nicolini, G., Noormets, A., Northwood, M., Nosetto, M., Nouvellon, Y., Novick, K., Oechel, W., Olesen, J.E., Ourcival, J.-M., Papuga, S.A., Parmentier, F.-J., Paul-Limoges, E., Pavelka, M., Peichl, M., Pendall, E., Phillips, R.P., Pilegaard, K., Pirk, N., Posse, G., Powell, T., Prasse, H., Prober, S.M., Rambal, S., Rannik, Ü., Raz-Yaseef, N., Rebmann, C., Reed, D., Dios, V.R.d., Restrepo-Coupe, N., Reverter, B.R., Roland, M., Sabbatini, S., Sachs, T., Saleska, S.R., Sánchez-Cañete, E.P., Sanchez-Mejia, Z.M.,

Schmid, H.P., Schmidt, M., Schneider, K., Schrader, F., Schroder, I., Scott, R.L., Sedlák, P., Serrano-Ortíz, P., Shao, C., Shi, P., Shironya, I., Siebicke, L., Šigut, L., Silberstein, R., Sirca, C., Spano, D., Steinbrecher, R., Stevens, R.M., Sturtevant, C., Suyker, A., Tagesson, T., Takanashi, S., Tang, Y., Tapper, N., Thom, J., Tomassucci, M., Tuovinen, J.-P., Urbanski, S., Valentini, R., van der Molen, M., van Gorsel, E., van Huissteden, K., Varlagin, A., Verfaillie, J., Vesala, T., Vincke, C., Vitale, D., Vygodskaya, N., Walker, J.P., Walter-Shea, E., Wang, H., Weber, R., Westermann, S., Wille, C., Wofsy, S., Wohlfahrt, G., Wolf, S., Woodgate, W., Li, Y., Zampedri, R., Zhang, J., Zhou, G., Zona, D., Agarwal, D., Biraud, S., Torn, M., Papale, D., 2020. The FLUXNET2015 dataset and the ONEFlux processing pipeline for eddy covariance data. Sci Data 7 (1), 225.

Ragab, R., Evans, J.G., Battilani, A., Solimando, D., 2017. The cosmic-ray soil moisture observation system (Cosmos) for estimating the crop water requirement: new approach. Irrigation and drainage 66 (4), 456–468.

Rasche, D., Köhli, M., Schrön, M., Blume, T., Güntner, A., 2021. Towards disentangling heterogeneous soil moisture patterns in cosmic-ray neutron sensor footprints. Hydrol. Earth. Syst. Sci. 25 (12), 6547–6566.

Rasche, D., Weimar, J., Schrön, M., Köhli, M., Morgner, M., Güntner, A., Blume, T., 2023. A change in perspective: downhole cosmic-ray neutron sensing for the estimation of soil moisture. Hydrol. Earth. Syst. Sci. 27 (16), 3059–3082.

Rebmann, C., Aubinet, M., Schmid, H., Arriga, N., Aurela, M., Burba, G., Clement, R., De Ligne, A., Fratini, G., Gielen, B., 2018. ICOS eddy covariance flux-station site setup: a review. Int. Agrophys. 32 (4), 471–494.

Reichenau, T.G., Korres, W., Schmidt, M., Graf, A., Welp, G., Meyer, N., Stadler, A., Brogi, C., Schneider, K., 2020. A comprehensive dataset of vegetation states, fluxes of matter and energy, weather, agricultural management, and soil properties from intensively monitored crop sites in Western Germany. Submitted to Earth System Science Data.

Rivera Villarreyes, C., Baroni, G., Oswald, S.E., 2011. Integral quantification of seasonal soil moisture changes in farmland by cosmic-ray neutrons. Hydrol. Earth. Syst. Sci. 15 (12), 3843–3859.

Rosolem, R., Hoar, T., Arellano, A., Anderson, J.L., Shuttleworth, W.J., Zeng, X., Franz, T.E., 2014. Translating aboveground cosmic-ray neutron intensity to high-frequency soil moisture profiles at sub-kilometer scale. Hydrol. Earth. Syst. Sci. 18 (11), 4363–4379.

Rosolem, R., Shuttleworth, W.J., Zreda, M., Franz, T.E., Zeng, X., Kurc, S.A., 2013. The effect of atmospheric water vapor on neutron count in the cosmic-ray soil moisture observing system. J. Hydrometeorol. 14 (5), 1659–1671.

Rudolph, S., van der Kruk, J., Von Hebel, C., Ali, M., Herbst, M., Montzka, C., Pätzold, S., Robinson, D.A., Vereecken, H., Weihermüller, L., 2015. Linking satellite derived LAI patterns with subsoil heterogeneity using large-scale ground-based electromagnetic induction measurements. Geoderma 241, 262–271.

Saby, N., Loubet, B., Winck, B., Ghebler Goydarag, M., Papale, D., Arrouays, D., Lafont, S.. Computing C stock for one ICOS site. https://www.swissfluxnet.ethz.ch/wp-content/uploads/2024/02/CH-DavCarbonReportv2_ICOS_20231025.pdf.

Schattan, P., Baroni, G., Oswald, S.E., Schöber, J., Fey, C., Kormann, C., Huttenlau, M., Achleitner, S., 2017. Continuous monitoring of snowpack dynamics in alpine terrain by aboveground neutron sensing. Water Resour Res 53 (5), 3615–3634.

Schattan, P., Schwaizer, G., Schöber, J., Achleitner, S., 2020. The complementary value of cosmic-ray neutron sensing and snow covered area products for snow hydrological modelling. Remote Sens Environ 239, 111603.

Schmidt, M., Becker, N., Becker, N., Dolfus, D., Esser, O., Graf, A., Kettler, M., Kummer, S., Mattes, J., 2023. ETC L2 ARCHIVE, Selhausen Juelich, 2018-12-31–2023-09-30, Ecosystem Thermatic Centre. https://meta.icos-cp.eu/objects/URRZy5sWnt7cHjsxEeMs0Ceb.

Schmidt, M.a.B., Becker, Shirin, Dolfus, Nils, Esser, Daniel, Graf, Odilia, Haustein, Alexander, Kettler, Andreas, Kummer, Martina, Mattes, Sirgit, Judith, 2024. ETC L2 ARCHIVE, Selhausen Juelich, 2019-01-01–2024-10-01. Ecosystem Thematic Centre.

Schrön, M., Köhli, M., Scheiffele, L., Iwema, J., Bogena, H.R., Lv, L., Martini, E., Baroni, G., Rosolem, R., Weimar, J., 2017. Improving calibration and validation of cosmic-ray neutron sensors in the light of spatial sensitivity. Hydrol. Earth. Syst. Sci. 21 (10), 5009–5030.

Schrön, M., Köhli, M., Zacharias, S., 2022. Signal contribution of distant areas to cosmic-ray neutron sensors - implications on footprint and sensitivity. EGUsphere 2022, 1–25.

Schrön, M., Rasche, D., Weimar, J., Köhli, M., Herbst, K., Boehrer, B., Hertle, L., Kögler, S., Zacharias, S., 2024. Buoy-based detection of low-energy cosmic-ray neutrons to monitor the influence of atmospheric, geomagnetic, and heliospheric effects. Earth and Space Science 11 (6) e2023EA003483.

Schrön, M., Zacharias, S., Womack, G., Köhli, M., Desilets, D., Oswald, S.E., Bumberger, J., Mollenhauer, H., Kögler, S., Remmler, P., 2018. Intercomparison of cosmic-ray neutron sensors and water balance monitoring in an urban environment. Geoscientific Instrumentation, Methods and Data Systems 7 (1), 83–99.

Serrano, J.M., Shahidian, S., Marques da Silva, J.R., 2016. Monitoring pasture variability: optical OptRx® crop sensor versus Grassmaster II capacitance probe. Environ Monit Assess 188, 1–17.

Shuttleworth, J., Rosolem, R., Zreda, M., Franz, T., 2013. The COsmic-ray Soil moisture Interaction Code (COSMIC) for use in data assimilation. Hydrol. Earth. Syst. Sci. 17 (8), 3205–3217.

Slingo, J.M., Challinor, A.J., Hoskins, B.J., Wheeler, T.R., 2005. Introduction: food crops in a changing climate. Philosophical Transactions of the Royal Society B: Biological Sciences 360 (1463), 1983–1989.

Tardieu, F., 2022. Different avenues for progress apply to drought tolerance, water use efficiency and yield in dry areas. Curr. Opin. Biotechnol. 73, 128–134.

ten Harkel, J., Bartholomeus, H., Kooistra, L., 2019. Biomass and crop height estimation of different crops using UAV-based LiDAR. Remote Sens (Basel) 12 (1), 17.

Thoele, H., Ehlert, D., 2010. Biomass related nitrogen fertilization with a crop sensor. Appl Eng Agric 26 (5), 769–775.

Tian, Z., Li, Z., Liu, G., Li, B., Ren, T., 2016. Soil water content determination with cosmic-ray neutron sensor: correcting aboveground hydrogen effects with thermal/fast neutron ratio. J Hydrol 540, 923–933.

Togliatti, K., Hornbuckle, B.K., 2018. Using a cosmic-ray neutron sensor (CRNS) to monitor vegetation. In: IGARSS 2018-2018 IEEE International Geoscience and Remote Sensing Symposium. IEEE, pp. 7365–7368.

Topp, G.C., Davis, J.L., Annan, A.P., 1980. Electromagnetic determination of soil water content: measurements in coaxial transmission lines. Water Resour Res 16 (3), 574–582.

Vitale, D., Fratini, G., Bilancia, M., Nicolini, G., Sabbatini, S., Papale, D., 2020. A robust data cleaning procedure for eddy covariance flux measurements. Biogeosciences. 17 (6), 1367–1391.

Wagner, W., Blöschl, G., Pampaloni, P., Calvet, J.-C., Bizzarri, B., Wigneron, J.-P., Kerr, Y., 2007. Operational readiness of microwave remote sensing of soil moisture for hydrologic applications. Hydrology Research 38 (1), 1–20.

Walker, J.P., Houser, P.R., Willgoose, G.R., 2004. Active microwave remote sensing for soil moisture measurement: a field evaluation using ERS-2. Hydrol Process 18 (11), 1975–1997.

Wang, L., Wang, P., Liang, S., Qi, X., Li, L., Xu, L., 2019. Monitoring maize growth conditions by training a BP neural network with remotely sensed vegetation temperature condition index and leaf area index. Comput. Electron. Agric. 160, 82–90.

Wang, X., Singh, D., Marla, S., Morris, G., Poland, J., 2018. Field-based high-throughput phenotyping of plant height in sorghum using different sensing technologies. Plant Methods 14 (1), 1–16.

Watanabe, K., Guo, W., Arai, K., Takanashi, H., Kajiya-Kanegae, H., Kobayashi, M., Yano, K., Tokunaga, T., Fujiwara, T., Tsutsumi, N., 2017. High-throughput phenotyping of sorghum plant height using an unmanned aerial vehicle and its application to genomic prediction modeling. Front Plant Sci 8, 421.

Weihermüller, L., Huisman, J., Lambot, S., Herbst, M., Vereecken, H., 2007. Mapping the spatial variation of soil water content at the field scale with different ground penetrating radar techniques. J Hydrol 340 (3-4), 205–216.

Western, A.W., Grayson, R.B., Blöschl, G., 2002. Scaling of soil moisture: A hydrologic perspective. Annu Rev Earth Planet Sci 30 (1), 149–180.

Wilhelm, W., Ruwe, K., Schlemmer, M.R., 2000. Comparison of three leaf area index meters in a corn canopy. Crop Sci. 40 (4), 1179–1183.

Wutzler, T., Lucas-Moffat, A., Migliavacca, M., Knauer, J., Sickel, K., Šigut, L., Menzer, O., Reichstein, M., 2018. Basic and extensible post-processing of eddy covariance flux data with REddyProc. Biogeosciences. 15 (16), 5015–5030.

Zheng, Y., Coxon, G., Woods, R., Power, D., Rico-Ramirez, M.A., McJannet, D., Rosolem, R., Li, J., Feng, P., 2023. Evaluation of reanalysis soil moisture products using Cosmic ray neutron Sensor observations across the globe. Hydrology and Earth System Sciences Discussions 2023, 1–27.

Zhu, Z., Tan, L., Gao, S., Jiao, Q., 2014. Observation on soil moisture of irrigation cropland by cosmic-ray probe. IEEE Geoscience and Remote Sensing Letters 12 (3), 472–476.

Zreda, M., Desilets, D., Ferré, T.P.A., Scott, R.L., 2008. Measuring soil moisture content non-invasively at intermediate spatial scale using cosmic-ray neutrons. Geophys Res Lett 35 (21).

Zreda, M., Shuttleworth, W.J., Zeng, X., Zweck, C., Desilets, D., Franz, T., Rosolem, R., 2012. COSMOS: the cosmic-ray soil moisture observing system. Hydrol. Earth. Syst. Sci. 16 (11), 4079–4099.

Zacharias, S., Loescher, H.W., Bogena, H., Kiese, R., Schrön, M., Attinger, S., Blume, T., Borchardt, D., Borg, E., Bumberger, J., Chwala, C., Dietrich, P., Fersch, B., Frenzel, M., Gaillardet, J., Groh, J., Hajnsek, I., Itzerott, S., Kunkel, R., Kunstmann, H., Kunz, M., Liebner, S., Mirtl, M., Montzka, C., Musolff, A., Pütz, T., Rebmann, C., Rinke, K., Rode, M., Sachs, T., Samaniego, L., Schmid, H.P., Vogel, H. J., Weber, U., Wollschläger, U., Vereecken, H., 2024. Fifteen years of integrated terrestrial environmental observatories (TERENO) in Germany: Functions, services, and lessons learned. Earth's Future 12 (6), e2024EF004510.